N-Substituted 5-(1H-Indol-2-yl)-2-methoxyanilines are Allosteric Inhibitors of the Linoleate Oxygenase Activity of Selected Mammalian ALOX15 Orthologs: Mechanism of Action

Alexey Golovanov[†#], Alexander Zhuravlev[†#], Alejandro Cruz[‡], Vladislav Aksenov[†], Rania Shafiullina[†], Kumar R. Kakularam[§], José M. Lluch[‡,∥], Hartmut Kuhn[§], Àngels González-Lafont[‡,∥] and Igor Ivanov[†*]

[†]Lomonosov Institute of Fine Chemical Technologies, MIREA - Russian Technological University, Vernadskogo Pr. 86, 119571 Moscow, Russia

[‡]Departament de Química, Universitat Autònoma de Barcelona, 08193 Bellaterra, Barcelona, Spain

[§]Department of Biochemistry, Charite - University Medicine Berlin, Corporate member of Free University Berlin, Humboldt University Berlin and Berlin Institute of Health Charitéplatz 1, D-10117 Berlin, Germany

[∥]Institut de Biotecnologia i de Biomedicina (IBB), Universitat Autònoma de Barcelona, 08193 Bellaterra, Barcelona, Spain

ABSTRACT: Here we describe the first systematic study on the mechanism of substrate selective inhibition of mammalian ALOX15 orthologs. For this purpose we prepared a series of *N*-substituted 5-(1H-indol-2-yl)anilines and found that (*N*-(5-(1H-indol-2-yl)-2-methoxyphenyl)sulfamoyl)carbamates and their monofluorinated analogues are potent and selective inhibitors of the linoleate oxygenase activity of rabbit and human ALOX15. Introduction of a 2-methoxyaniline moiety into the core pharmacophore plays a crucial role for substrate selective inhibition of ALOX15-catalyzed oxygenation of linoleic acid at submicromolar concentrations without affecting arachidonic acid oxygenation. Steady state kinetics, mutagenesis studies and molecular dynamics simulations suggested an allosteric mechanism of action. Using a dimer model of ALOX15 our MD-simulations suggest that binding of the inhibitor at the active site of one monomer induces conformational alterations in the other monomer so that the formation of a productive enzyme-linoleic acid complex is energetically compromised.

KEYWORDS: 5-(1H-indol-2-yl)-2-methoxyanilines, lipoxygenase inhibitors, allosterism, protein–protein interactions, molecular dynamics

INTRODUCTION

Lipoxygenases form a family of lipid peroxidizing enzymes that have been implicated in cell differentiation,[1-3] in the pathogenesis of inflammatory and anaphylactic diseases,[4-8] in atherogenesis,[9-10] in ferroptosis,[11-12] in insulin resistance and in adipose tissue inflammation, which is a key element of obesity.[13-15] In humans there are six functional LOX genes (ALOX15, ALOX15B, ALOX12, ALOX12B, ALOX5, ALOXE3) and their expression leads to the formation of six functionally distinct ALOX-isoforms. One of these enzymes, ALOX15, is somewhat peculiar because of its capability of oxygenating complex lipid-protein assemblies such as biomembranes and lipoproteins[16] and the emerging role of this isoenzyme in human pathologies has recently been reviewed[17]. In inflammation ALOX15 exhibits dual functionality[18]. In various inflammation models ALOX15 products induced pro-inflammatory effects. On the other hand, reports suggesting anti-inflammatory activities of ALOX15 orthologs challenged the strategy of developing ALOX15 inhibitors for the treatment of human diseases.[19-21]

The putative pathophysiological roles of ALOX15 made this enzyme a target for pharmacological research. A number ALOX15 inhibitors that have been developed in the past involve nitrogen containing heterocycles. Among them are highly potent oxadiazole or oxazole derivatives,[22] pyrazole-based sulfonamides and sulfamides,[23] imidazol-based sulfonamide analogs,[24] indole-based inhibitors[25-28] as well as tryptamine sulfonamides[29]. Most of these compounds inhibit ALOX15-catalyzed oxygenation of linoleic acid (LA) with a similar efficiency as arachidonic acid conversion.[24, 29] However, for some compounds their inhibitory potency depends on the fatty acid substrate[29] and this substrate specific inhibition may be of biological relevance. In fact,

substrate specific ALOX inhibitors may impact the formation of deleterious linoleic acid derived mediators without impacting the biosynthesis of beneficial signalling molecules formed from other polyenoic fatty acids. When we tested isobuthyl (*N*-(5-(5,6-difluoro-1H-indol-2-yl)-2-methoxyphenyl)sulfamoyl)carbamate[26] as inhibitor for purified human ALOX15 we observed selective inhibition of the linoleate oxygenase activity of the enzyme with an IC_{50}(LA)/IC_{50}(AA) ratio of 0.03 (SI **Figure S1**). The observed difference could not be explained by the conventional one ligand-binding model,[30] in which inhibitor and substrates compete for binding at the catalytic centre of the monomeric enzyme. Since rabbit ALOX15 may occur as non-covalent dimer in aqueous solution[31-32], such weak intermolecular association may contribute to the allosteric character.[33-34]

To explore the molecular basis for substrate-specific inhibition of the linoleate-oxygenase activity of ALOX15 by isobuthyl (*N*-(5-(5,6-difluoro-1H-indol-2-yl)-2-methoxyphenyl)sulfamoyl)carbamate[26] we first performed *in silico* docking studies to fit the compound into the substrate binding pocket of rabbit ALOX15. Since no crystal data is currently available for human ALOX15 most of our mechanistic experiments were carried out with rabbit ALOX15. After the initial docking studies we selected (N-(3-(1H-indol-2-yl)phenyl)sulfamoyl)carbamic acid as core pharmacophore, prepared a set of modified analogues and tested their activities against rabbit, human and mouse recombinant mammalian ALOX15 orthologs. Considering our previous finding that docking of arachidonic acid (AA) into the active site of conformer A of rabbit ALOX15 resulted in an unstable enzyme-substrate complex (unpublished data), we used a new dimer model for rabbit ALOX15, in which the substrate binding pocket of conformer A is occupied by the inhibitor, whereas conformer B involved the substrate fatty acid at its catalytic centre. Finally, we performed site-directed mutagenesis studies and MD simulations to explore the consequences of inhibitor binding on substrate alignment at the active site of the other monomer.

RESULTS

Targeted drug design and structure activity relation (SAR). In aqueous solutions rabbit ALOX15 exhibits a conformational heterogenity[35] and is present in a dynamic equilibrium between monomeric and dimeric fractions at physiological salt concentrations[31]. Although the allosteric character of ALOX15 was first reported more than a decade ago[33], the precise mechanism of allosteric regulation of the enzyme remains elusive. Thus, it was impossible to create powerful allosteric inhibitors employing the conventional methods of rational drug design. On the other hand, a literature search for ALOX15 inhibitors revealed that only for a limited number of compounds the IC_{50}(LA)/IC_{50}(AA) ratios has been determined in the past[23, 29]. For the present study we quantified the IC50 values for isobuthyl (*N*-(5-(5,6-difluoro-1H-indol-2-yl)-2-methoxyphenyl)sulfamoyl)carbamate for linoleic acid and arachidonic acid oxygenation by the pure recombinant human ALOX15 (SI **Figure S1**) and obtained a ratio of 0.03 (**Figure 1A**). The imidazole based N-(2-(5-(4-methoxyphenyl)-2-(pyridin-2-yl)-1H-imidazol-4-yl)ethyl)-4-pentylbenzenesulfonamide (**Figure 1B**)[24] exhibited a similar degree of substrate specific inhibition for rabbit ALOX15. Interestingly, 3-substitution at the indole ring (**Figure 1C**) reduced the degree of substrate selectivity of the inhibitor against rabbit ALOX15 and the absence of a methoxyaryl moiety completely abolished substrate specific inhibition.[29] Based on this data one might conclude that a 2-methoxyaniline moiety attached to position C2 of the core pharmacophore may play a crucial role for the degree of substrate specific inhibition of the linoleate oxygenase activity of ALOX15. When we carried out docking studies of the sulfamoylcarbamate depicted in **Figure 1A** into the putative substrate binding pocket of monomer A of the rabbit ALOX15 dimer (PDB entry 2PoM) we found that the inhibitor in its best docking pose is located in the hydrophobic substrate binding pocket of monomer A with its 5-(1H-indol-2-yl)-2-methoxyaniline motif ahead (SI **Figure S2**). The carbamic acid ester group was located close to the entrance of the substrate binding pocket of monomer A and partly interconnected the two monomers within the enzyme dimer. The NH2 groups of Arg599 and Arg403 interact electrostatically with the oxygen atom of the methoxy group and the NH2 group of Gln596 forms a hydrogen bond with that same oxygen atom. Finally, it is worth mentioning that one of the two fluorine atoms presents unfavourable electrostatic interactions with Glu357 (SI **Figure S2**).This binding mode suggests that the chemical nature of residues I, II and III (**Figure 1A**) might be of critical relevance for the allosteric properties of the inhibitor. On this basis three lines of modifications of the inhibitor have been suggested: i) Since OCH3-group of the methoxyaniline moiety may limit the mobility of this ligand inside the catalytic cavity we replaced this residue by a small hydrogen atom. ii) The binding mode of the inhibitor we identified during our docking studies offers sufficient space around the tail of carbamic acid ester moiety for chemical modification of substituent II. Thus, we reasoned that incorporation of a long chain aliphatic ester group at this position might increase the lipohylicity of this residue and, hence, might improve the binding affinity of

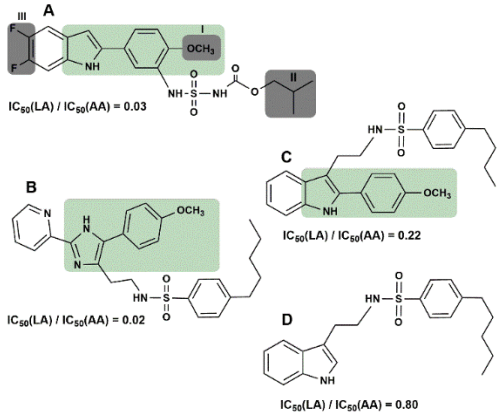

Figure 1. Selected structures of the substrate specific and non-specific ALOX15 inhibitors.

Scheme 1. Synthetic Route of compounds 6-8[a]

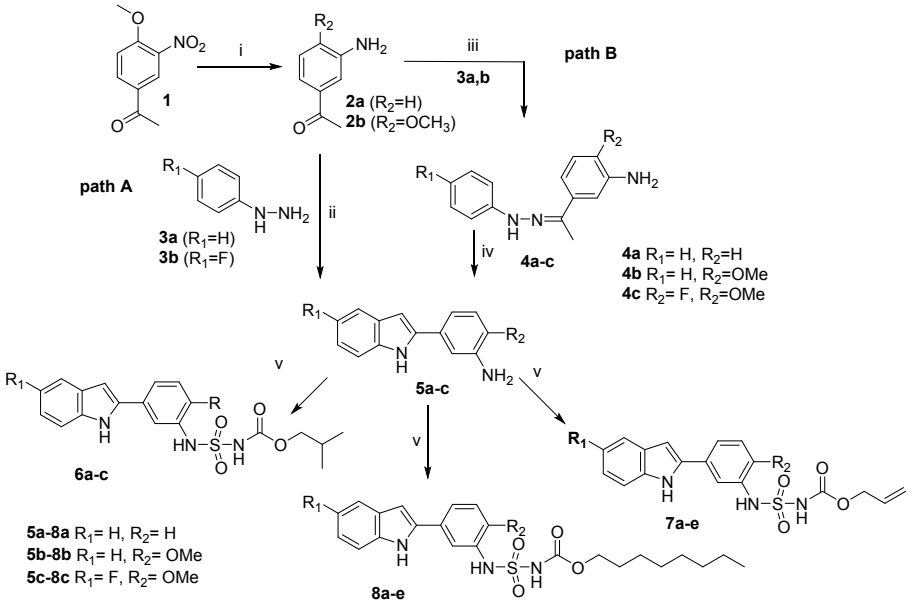

[a]Reagents and conditions: (i) 10% Pd/C, $HCOONH_4$, EtOH, reflux; (ii) PPA, 130 °C, 0.5h; (iii) AcOH, EtOH, reflux; (iv) $ZnCl_2$,180 °C, 2h; (v) $ClSO_2NCO$, $HN(C_2H_5)_2$, isobuthyl-, allyl - or octylalcohol, rt.

the inhibitor at the hydrophobic environment of the catalytic centre. Moreover, introduction of an allylic ester moiety may force additional π-π interactions between the inhibitor and aromatic active site amino acids and thus, may strengthen the protein-inhibitor interactionn. iii) Since fluorination of the indole ring may not only enhance the metabolic stability of the pharmacophore towards oxidation, but also might be important for the alignment of the inhibitor at the enzyme's active site, we also prepared non fluorinated and mono C5-fluorinated inhibitor derivatives.

Chemical synthesis of substituted N-(3-(1H-indol-2-yl)phenyl)sulfamoylcarbamates. To test the validity of our *in silico* predictions we synthesized a set of nine 2-arylindolderivatives involving the following precursors: 3-(1H-indol-2-yl)aniline (**5a**), 5-(1H-indol-2-yl)-2-methoxyaniline (**5b**) and its mono halogenated derivative **5c**. Previously reported methods for preparation of substituted 3-(1H-indol-2-yl)anilines employ the canonic Bischler-Möllau indol cyclization reaction[26-27]. Here were report that **5a-c** may be prepared *via* the Fischer indole synthesis using commercially available starting compounds (**Scheme 1**) in a one-pot procedure under solvent-free conditions. For the synthesis we used commercial phenylhydrazines **3**, 1-(3-aminophenyl)ethan-1-one (**2a**) or 1-(3-amino-4-methoxyphenyl)ethan-1-one (**2b**). The latter was prepared from the corresponding nitro derivative by reduction of NO_2-group using ammonium formiate in the presence of 10%-Pd/C catalyst. Next, we optimized the reaction conditions for compounds **2a-b** and **3a-b** using different Lewis acids. In our hands, under the previously described reaction conditions ($ZnCl_2$/180°C)[36] we observed the formation of a complex product mixture as concluded from HPLC and ^{1}H NMR analyses and unfortunately, the overall yields of the target 2-arylindoles **5a-c** did not exceed 10%. Similar results were obtained when the synthesis was performed according to a two-step procedure *via* isolation of the intermediate hydrazones **4a-c** (**Scheme 1**, Path B, for analytical data see supporting information). The low yields (5-10%) at the cyclization step of the corresponding hydrazone can be explained by the formation of a large number of side-products due to a relatively low reaction rate (2-5 h) and the high temperature (180°C). In contrast, in polyphosphoric acid (PPA)[37] all targeted 2-arylindoles were obtained at relatively high yields of 50-60% within 15-30 minutes at rather moderate temperatures (120°C-130°C) (**Scheme 1**, Path A). The physical data of compounds **5a** and **5b** were identical to those reported in the literature.[27, 38] The resulting indoles **5a-c** were subsequently transformed to the derivatives **6-8** by the reaction with chlorosulfoisocyanate and the corresponding alcohol in the presence of diethylamine.[26] As expected, in ^{13}C-NMR spectra of the fluorinated compounds **6c-8c** the signal of C5 (158 ppm) was split into a doublet with J = 232 Hz. In contrast, the signals of C4 and C6 at 105 and 110 ppm were split with lower coupling constants (J = 23.5 and 26 Hz, respectively; SI **Figure S3).**

Inhibitory potency of substituted (*N*-(3-(1H-indol-2-yl)-phenyl)sulfamoyl)carbamates 6-8 for ALOX15. During the first round of testing, we determined the IC_{50} values for nine compounds using the pure recombinant rabbit ALOX15 as target enzyme. Inhibition was measured employing the standard spectrophotometric assay monitoring the rate of conjugated diene formation when arachidonic or linoleic acids were used as substrates. The IC_{50} values varied between 0.04 for linoleic acid and >50 μM for

Table 1. Inhibitory activity of substituted 2-arylindolsulfocarbamates 6-8 against rabbit ALOX15.

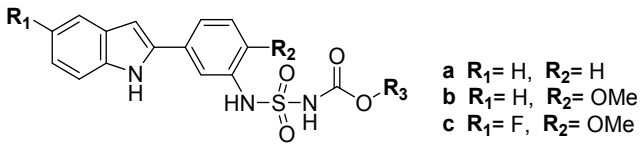

Indole Type	**6,** R_3= -CH_2-$CH(CH_3)_2$			**7,** R_3= -CH-$CH=CH_2$			**8,** R_3= -$(CH_2)_7$-CH_3		
	LA IC_{50}, μM[a]	AA IC_{50}, μM[a]	IC50LA/IC50AA ratio	LA IC_{50}, μM[a]	AA IC_{50}, μM[a]	IC50LA/IC50AA ratio	LA IC_{50}, μM[a]	AA IC_{50}, μM[a]	LA/AA ratio
a	29.97±12.20	> 50	> 0.60	15.38±10.20	> 50	> 0.30	1.55±0.34	2.79±1.53	0.55
b	1.45±0.27	> 50	> 0.030	0.63±0.32	43.34±13.09	0.014	0.040±0.001	2.06±0.14	0.020
c	0.42±0.03	20.82±2.12	0.020	0.54±0.06	23.26±3.46	0.023	0.047±0.001	1.08±0.06	0.043

[a]The data have been obtained on the basis of dose response curves for spectrophotometric ALOX15 activity assay for purified rabbit ALOX15 (see Experimental Section). All data represent means ± SEM of three independent (n=3) measurements.

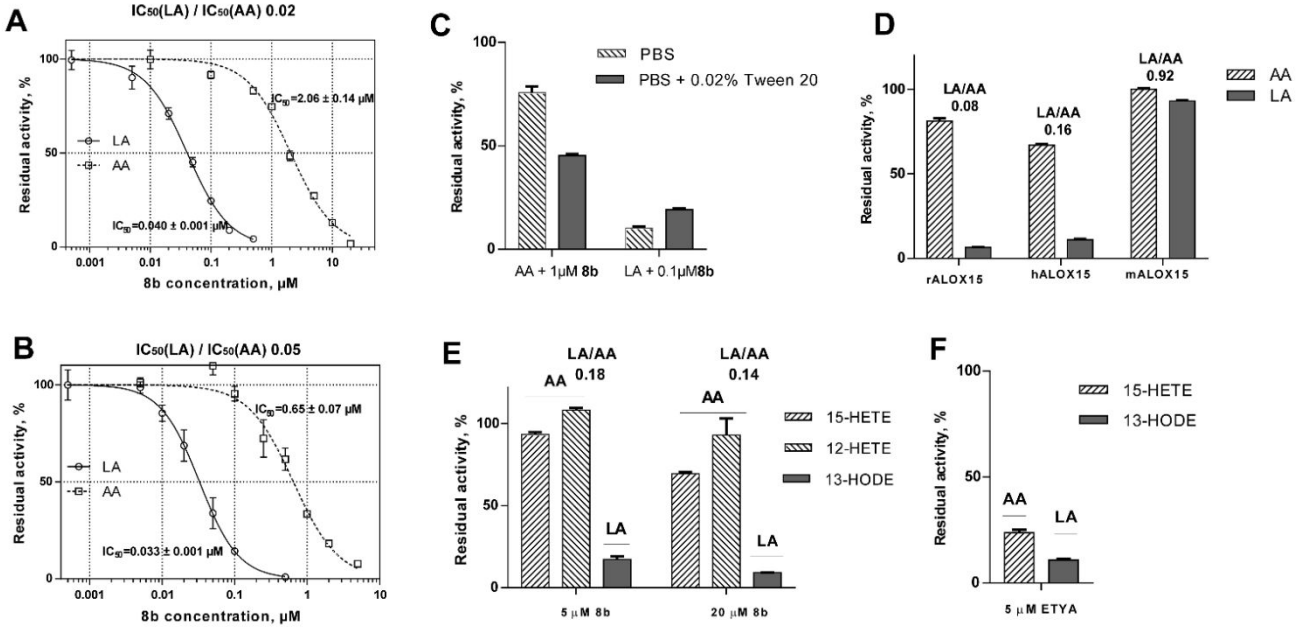

Figure 2. Dose response curves for inhibition of LA- and AA-oxygenase activities of mammalian ALOX15 orthologs. The LA- and AA oxygenase activities of pure recombinant rabbit (A) and pure recombinant human (B) ALOX15 orthologs were assayed in the presence or absence of compound **8b**. Spectrophotometric assay were performed a described in Experimental Section and half-maximal inhibitory concentrations (IC50) were determined. (C) Effect of detergent (Tween 20) on inhibitory potency of **8b** on rabbit ALOX15. Spectrophotometric assays were performed a described in Experimental Section. (D) Inhibition of different mammalian ALOX15 orthologs by **8b** using the HPLC-based activity assay. The assay was performed a described in Experimental Section .The ALOX activity of the incubation sample lacking the inhibitor was set 100%. Finally, we calculated the ratios of residual activities of LA oxygenation *vs.* AA oxygenation (formation of 13-HODE *vs.* formation of 15-HETE) as suitable measure for the substrate selectivity of the inhibitory effect. (E) Inhibition of the intracellular human ALOX15 by **8b** using L1236 Hodgkin lymphoma cells. The assay was performed a described in Experimental Section. The ALOX activity of the incubation sample lacking the inhibitor was set 100%. As suitable measure for the substrate selectivity of the inhibitory effect of **8b** we calculated the ratios of residual activities of LA oxygenation *vs.* AA oxygenation (formation of 13-HODE *vs.* formation of 15-HETE). (F) Inhibition of the intracellular human ALOX15 by 5μM ETYA using L1236 Hodgkin lymphoma cells as enzyme source. The assay was performed under strictly comparable conditions as described for compound **8b**. All data represent means ± SEM of n=3 measurements.

arachidonic acid (**Table 1,** SI **Figure S4**). Thus, a pronounced substrate specific enzyme inhibition was observed. Comparison of the data indicates that the presence of the methoxy group at C2 of the aniline moiety (indole types **b** and **c**) is important not only for the inhibitory potency but also for the substrate selectivity of

the inhibitory effect (IC_{50}(LA)/IC_{50}(AA) ratio < 0.05). Replacement of the butyl moiety (**6b-c**) with an allyl group (**7b-c**) resulted in a moderate change in inhibitory potency of the compounds. In contrast, introduction of a more lipophilic octyl residue (compounds **8b-c**) resulted in app. 10-fold increase the inhibitory potency. Modification of the indol ring at C5 (introduction of a fluorine atom, **6c-8c**) moderately improved the inhibitor potency against both fatty acids, but had no effect on the substrate selectivity of inhibition**.** In summary, with IC_{50} values of 0.04 μM compounds **8b (Figure 2A)** and **8c** appeared to be the same powerful as the best ALOX15 inhibitors described so far.[29] ML351, which has previously been identified as paralog-specific ALOX15 inhibitor was with an IC_{50} of 200 nM less potent.[39] It should be stressed at this point that the assay conditions used in the different literature studies and in our experiments were not strictly comparable (different enzyme preparations, different substrate concentrations, use of detergents) and thus, direct comparison of the determined IC_{50}-values may be misleading. However, most interestingly, compounds **6c**, **7b-c** and **8b** exhibited a high degree of substrate selectivity with IC_{50}(LA)/IC_{50}(AA) ratios varying between 0.014 and < 0.030 (**Table 1,** SI **Figure S4).** A similar trend for substrate specific inhibition was observed when **8b** was tested with recombinant human ALOX15 (**Figure 2B**).

Owing to their limited water solubility the activity of different inhibitors may depend on their aggregate state in aqueous solutions.[40] To exclude such physiologically irrelevant promiscuous effects we performed additional spectrophotometric inhibitor studies in PBS containing 0.02% Tween 20 solubilizer (0.1 and 1μM for LA and AA, respectively, **Figure 2C**). Here we found that substrate specific inhibition of ALOX15 was also seen in the presence of detergents (LA/AA ratio < 0.1). Since surface active compounds may also impact the enzyme structure we refrained from including detergents into the assay systems for the other experiments.

Next, we explored whether a similar substrate selective inhibition can be seen for mouse Alox15 ortholog. Since this enzyme could not be purified to homogenieity we employed crude enzyme preparations (bacterial lysate supernatants) for comparative experiments **(Figure 2D)** and a assayed the catalytic activities by a HPLC based system. Although enzyme inhibition was less pronounced when compared with our spectrophotometric assays a clear-cut substrate specific inhibition of rabbit and human ALOX15 was confirmed (**Figure 2D**). However, for mouse Alox15 no substrate selectivity could be detected. In fact, at 2 μM **8b** we hardly observed any inhibition of mouse Alox15 neither with LA nor with AA as substrate. These data suggest a pronounced ortholog specific inhibition of ALOX15 orthologs of different species by **8b**.

Finally, we tested whether the substrate specific inhibition of human ALOX15 can also be demonstrated in a cellular system. For this purpose we employed the Hodgkin lymphoma cells L1236, which constitutively express human ALOX15 at high levels.[41] These cells oxygenate AA to a mixture of 15-HpETE and 12-HpETE in the ratio 85:15 (**Figure 2E**), which is consistent with the product specificity of purified recombinant human ALOX15.[42] Although somewhat higher inhibitor concentrations were required to inhibit the cellular ALOX15 activity, preferential inhibition of the LA-oxygenase activity by **8b** was observed (LA/AA ratios 0.14-0.18) **(Figure 2E)**. On the other hand, the standard ALOX/COX inhibitor ETYA[43] did not show a major degree of substrate selectivity (**Figure 2F**). Taken together, these data indicate that the substrate-specific inhibitory effect of human ALOX15 by **8b** can also be observed for the intracellular enzyme.

Mechanism of inhibition. In order to explore the mechanism of the substrate-specific inhibition of the linoleate oxygenase activity of ALOX15 we employed compounds **6c** and **8b**, which exhibit low IC_{50}(LA)/LC_{50}(AA) ratios and carried out extensive kinetic measurements using pure recombinant rabbit ALOX15 (**Figure 3A-D**). The following kinetic constants were evaluated for this enzyme without inhibitor: k_{cat}^{LA}=32.5±1.0 s^{-1}, K_M^{LA}=24.5±5.0 μM, k_{cat}^{AA}=21.9.5±2.0 s^{-1}, K_M^{AA}=13.2±2.0 μM for LA and AA, respectively, and these data are consistent with our previous reports[42, 44]. Using LA as substrate both compounds (**6c** and **8b**) induced a marked decrease in k_{cat} but the K_M-values remained largely unaffected (SI **Figures S5 and S6**). Finally, we fitted these inhibitor data (**Figure 3A,C**) to different inhibition models and found that the best fits were obtained for a model of a non-competitive inhibition of LA oxygenation with a K_i of 21.9±0.5 nM (R^2= 0.977) for **8b** and K_i of 0.29±0.08 μM (R^2 = 0.985) for **6c**. For AA oxygenation **6c** and **8b** induced a marked decrease in both, k_{cat} and K_M values (SI **Figures S5 and S6**) and here the best fit of our experimental data was obtained for an uncompetitive mode of inhibition with a K_i of 0.95±0.06 μM (R^2 = 0.989) for **8b** and K_i of 6.53±0.49 μM (R^2 = 0.979) for **6c** (**Figure 3B,D**). On the other hand, inhibition of both substrates by the compound **8a** (SI **Figure S7**) could be equally well described by a mixed model of inhibition (R^2= 0.977) with a K_i of 0.79±0.02 μM (α=6.6) and 3.13±0.40 μM (α=7.9) for LA and AA, respectively. In this case the dissociation constant ratios K_d^{EI} to K_d^{ESI} of 0.075 and 0.153 for LA and AA, respectively, suggested a higher binding affinity of **8a** to the enzyme (E) rather than enzyme-substrate complex (ES).

Next, we tested the reversibility of **8b** induced inhibition of ALOX15 catalyzed LA oxygenation. For this purpose, a solution of pure rabbit ALOX15 was pre-incubated with a 100-fold molar excess of **8b** and activity assays suggested complete inhibition of the enzyme. Next, we removed the inhibitor by gel-filtration. The procedure was repeated several times until the final ratio of maximal UV-absorbance at 312 nm (inhibitor specific chromophore) *vs.* the absorbance of protein (280nm) remained constant (**Figure 3G**). The amount of inhibitor left in the pre-incubation mixture suggested that on average one protein molecule in the pre-incubation mixture binds one molecule of **8b**. However, activity assays using the spectrophotometric system

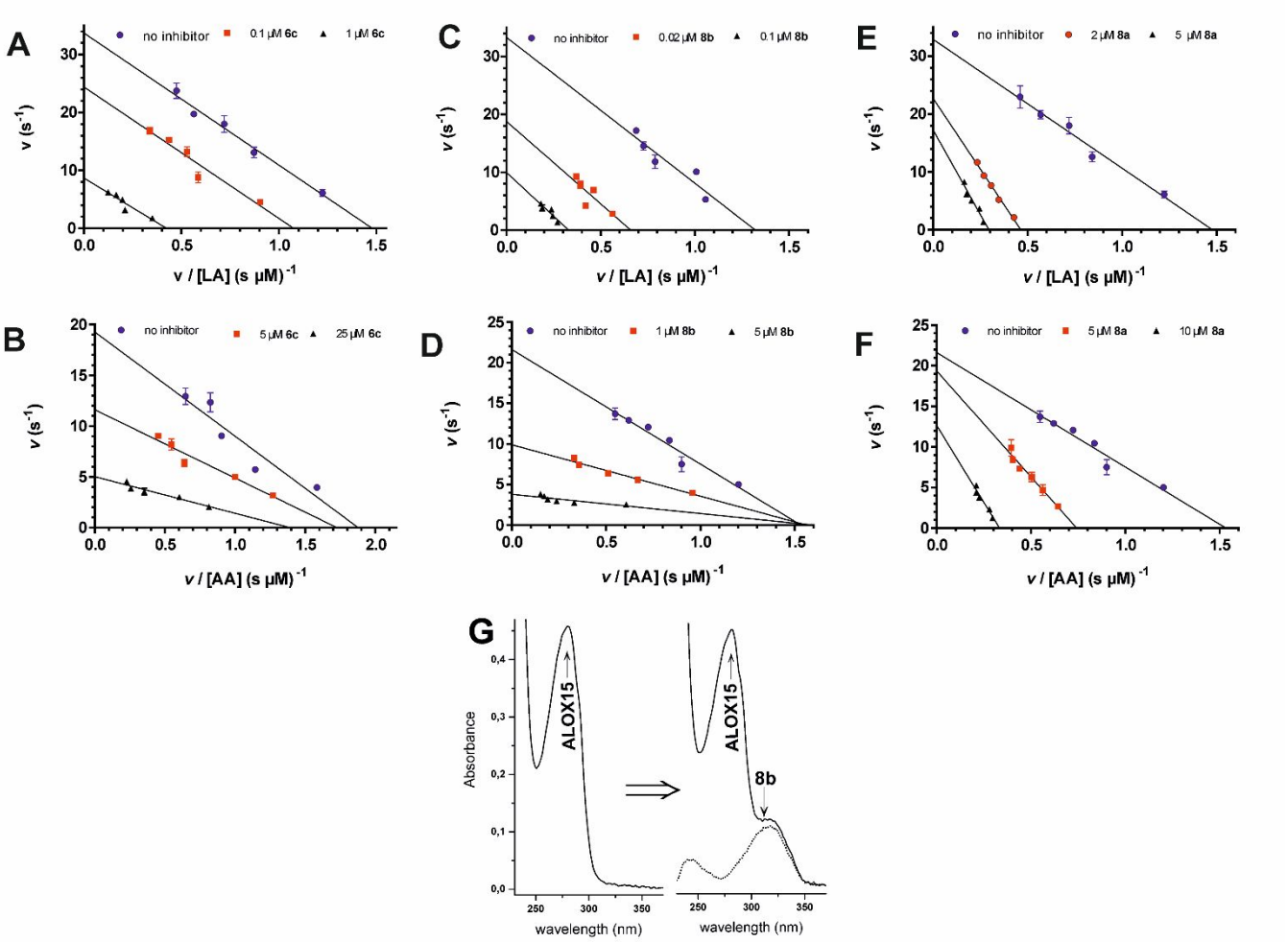

Figure 3. Mechanism of ALOX15 inhibition. (A-F) Eadie-Hofstee plots demonstrating the effects of **6c**, **8b** and **8a** on rabbit ALOX15 when incubated with 25 µM linoleic (A, C, E) or arachidonic (B, D, F) acids. Incubations were repeated at different inhibitor concentrations. All data points represent means ± SEM with n=3. (G) On average 1 molecule of **8b** binds to 1 molecule of rabbit ALOX15. To estimate the rALOX15:**8b** ratio molecular extinction coefficient of 1.78 $mg^{-1}cm^{-1}$ (280 nm) for the enzyme was used.

indicated almost complete recovery of the catalytic activity and thus, a reversible mode of action was concluded. Similar data were obtained with the compound **6c** (data not shown).

In general, sulfamoylcarbamates may undergo degradation in acidic aqueous solutions in the presence of Fe^{3+} (SI **Figure S8A-D**). This reaction is associated with a reduction of Fe^{3+} ions to the divalent ferrous form. Since no inhibitor degradation occurs during enzymatic catalysis with either substrate (AA or LA) (SI **Figure S8E**), one may exclude substrate specific decomposition reactions of the inhibitor. Moreover, preincubation of the ALOX15-**8b** complex with large amounts of organic peroxydes (13-HpODE, 20 µM) did neither impact the inhibitory activity (data not shown). These data exclude that substrate-specific enzyme inhibition may be related to the redox properties of the inhibitors.

Taken together, our data indicate that compounds **8b** and **6c** inhibit LA and AA oxygenation by rabbit ALOX15 in a reversible manner via different allosteric mechanisms. In contrast, **8a** tends to compete with both substrates for the substrate binding site (**Figure 3E,F**).

Effect of inhibitors on ALOX15 product pattern. Human and rabbit ALOX15 exhibit dual reaction specificity and arachidonic acid is converted by these two enzymes to a mixture of 15- and 12-HETE (90:10 for human and 95:5 for rabbit enzyme). Next, we explored whether **8a** and **8b** alter the reaction specificity of the rabbit enzyme. We found that both inhibitors do not modify the product pattern of AA oxygenation even at high inhibitor concentrations. Independent on the inhibitor concentration in the assay mixture we always quantified a 15-HETE / 12-HETE ratio of 95.5±0.2% / 4.5±0.2% (SI **Figure S9A**, left columns). A similar product pattern has previously reported for this enzyme in the absence of any inhibitor[45].However, **8b** induced subtle alterations in the product specificity of LA oxygenation (SI **Figure S9B**). When we applied the AA 12-lipoxygenating Ile418Ala mutant of rabbit ALOX15[46] for comparative experiments (SI **Figure S9A**, middle columns) we confirmed that this enzyme variant oxygenated AA predominantly to 12-HETE. Only a minor share (25 %) of

15-HETE formation was detected and the presence of **8a** did not alter this product pattern. However, **8b** reduced the relative share of 12-HETE formation when compared with the no inhibitor control (SI **Figure S9A**, middle columns). Here again, the inhibitor-induced alterations in the product specificity were rather subtle but statistically significant. With human ALOX15 as catalyst we observed that both **8a** and **8b** reduced the relative share of the major oxygenation product (15S-HETE) when compared with no-inhibitor controls (SI **Figure S9A**, right columns). The differences observed between rabbit and human ALOX15 may result from the structural differences of both enzymes, which share 71% of amino acid sequence identity. Taken together, these data show that inhibitor induces rather subtle but statistically significant alterations in the product specificity of ALOX15 that may be regarded as indication for enzyme-inhibitor interaction.

Leu183Glu+Leu192Glu mutation converts the effect of 8b on LA oxygenation to that of 8a. In a previous report we have shown that Leu183 and Leu192, which are oriented outwards the monomeric protein molecules, are important for the integrity of the inter-monomer interface of the ALOX15 dimer observed in the crystal structure (PDB ID 2PoM). Mutation of these residues to negatively charged glutamates (Leu183Glu+Leu192Glu mutant) affected the mode of self-association of the enzyme and this alteration was mirrored by modified catalytic properties (substrate inhibition above 10 μM)[44]. In this study we created a structural *in silico* model for the Leu183Glu+Leu192Glu double mutant of rabbit ALOX15 and performed a 200 ns MD simulation. The results show that His585(A), Trp181(B), and His585(B) form a network of π-π interactions even though this is rather weak. The hydrophobic amino acid cluster that stabilizes the inter-monomer interaction of the wild-type enzyme has been dismounted. In the double mutant Leu188 (B) was moved away and pointed outwards. Leu179 (A) did also moved away but pointed inwards the interface. Glu183 (A) and Glu192 (B) formed a salt bridge with Lys189 (B). Trp181 (A) moved outwards and did not contribute any more to the intermonomer interaction. In the wild-type ALOX15 dimer the α2(A) and α2(B) helices are located parallel, while in the Leu183Glu+ Leu192Glu double mutant they are not parallel any more (**Figure 4A,B**).

To obtain experimental evidence whether the effect of **8b** binding to one ALOX15 monomer may be translated to another LA-bound monomer via joint interface observed in the crystal structure we compared the inhibitor efficiency of compounds **8a** and **8b** on the LA- and AA-oxygenase activity of wild-type rabbit ALOX15 and its Leu183Glu+Leu192Glu double mutant. If allosteric mechanisms are involved in the mode of action of **8b** the Leu183Glu+Leu192Glu exchange should induce a right-shift of the dose-response curve of **8b** approaching that of compound **8a**. When we performed this experiment, we found that the dose response curves of LA and AA inhibition by **8b** were close to each other (**Figure 4C**) with IC_{50} values of 4.95±0.38 μM and 7.02±0.91 μM for AA and LA, respectively. In fact, the dose-response curves for **8b**(LA) and **8a**(LA) were almost identical. These data suggest that the structural integrity of the inter-monomer interface within the wild-type ALOX15 dimer may play a critical role for substrate specific inhibition of ALOX15 orthologs by **8b** (**Figure 4**).

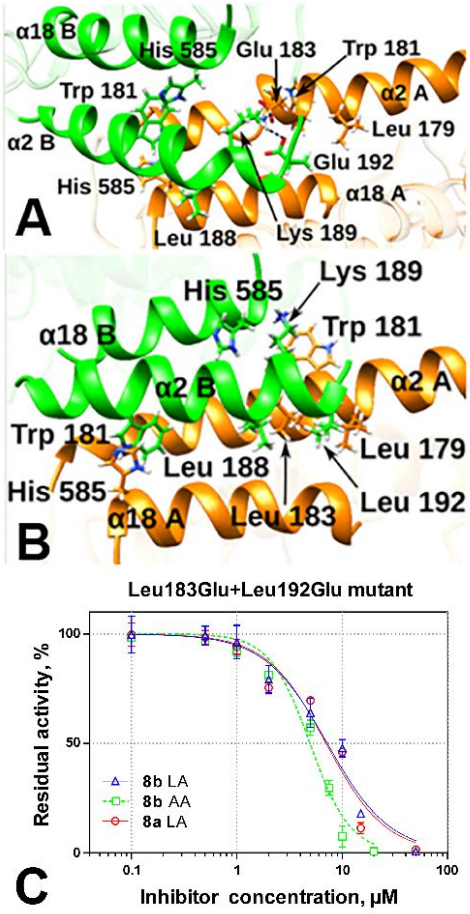

Figure 4. Leu183Glu+Leu192Glu mutant interface (A) vs. that of the wild-type enzyme (B). (C) Inhibition of linoleate and arachidonate oxygenase activity of rabbit ALOX15 L183E+L192E mutant (10 μg purified enzyme, 15 μM LA) in the presence of **8a** and **8b**. Spectrophotometric assays were performed as described in Experimental section. PDB ID 2PoM of crystal structures of rabbit ALOX15 was used as starting points for molecular modeling.

MD simulations of enzyme-inhibitor-substrate complexes. To explain the observation that compound **8b** induces substrate selective enzyme inhibition but **8a** does not (**Figures 2 and3**), we hypothesized that inhibitor binding at one monomer of the ALOX15 dimer may induce conformational alterations in the other monomer, which modifies the alignment of the fatty acid substrate at the active site. To test this hypothesis, we carried out MD simulations and employed a structural model, in which compounds **8a** and **8b** were placed inside the putative substrate binding pocket of conformer A and LA in the substrate binding pocket of conformer B [complexes ALOX15-8a(A)-LA(B), ALOX15-8b(A)-LA(B)] by means of docking calculations. Finally, we selected the energetically most favourable binding poses and initiated an MD trajectory. When LA was

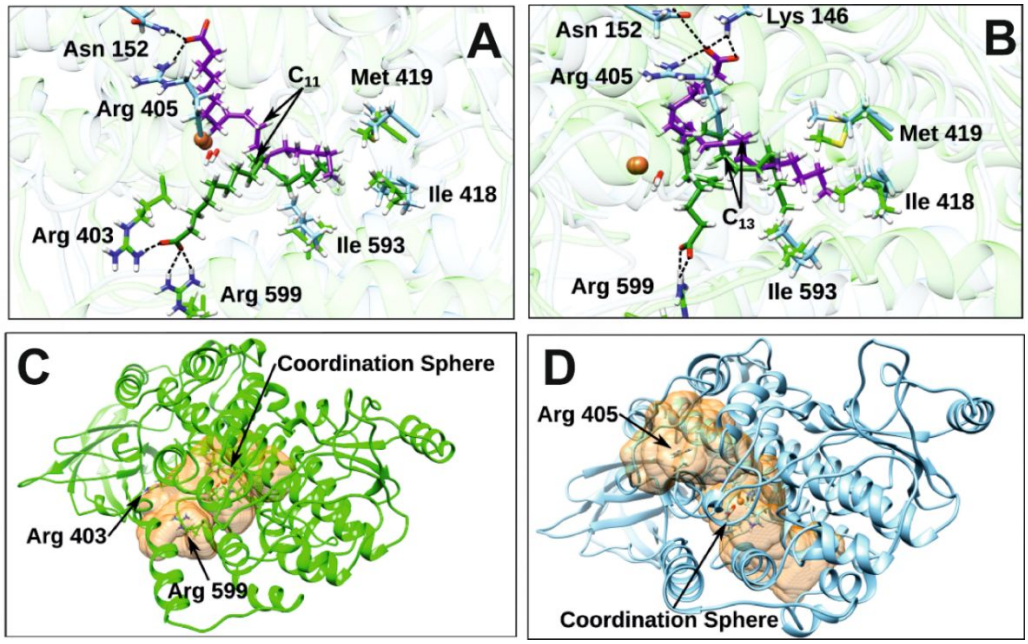

Figure 5. Effect of inhibitor on the substrate binding. (A) Most representative binding mode of LA in the ALOX15-**8a**(A)-LA(B) (in green) and ALOX15-**8b**(A)-LA(B) (in purple) complexes. (B) Most representative binding mode of AA in the ALOX15-**8a**(A)-AA(B) (in green) and ALOX15-8b(A)-AA(B) (in purple) complexes. The centroids of the most representative cluster for LA of the ALOX15-**8a**(A)-LA(B) and AA of the ALOX15-**8a**(A)-AA(B) complex simulation is depicted. The clustering has been carried out using an RMSD of 0.5 Å for the heavy atoms of the LA (AA) substrate**.** (C) Cavity surfaces of monomer B in ALOX15-8a(A)-LA(B) and (D) ALOX15-8b(A)-LA(B) complexes. Plots were carried out with the CavityPlus web server. PDB ID 2PoM of crystal structures of rabbit ALOX15 was used as starting points for molecular modeling.

bound at the conformer B in the ALOX15-**8a**(A)-LA(B) complex the most stable interactions along the MD between **8a** and the protein were a hydrogen bond of the side chain of Arg403 with the carbonyl moiety of **8a**. Another hydrogen bond was visible between the backbone oxygen atom of Arg403 and the NH-group of substituted aniline moiety of **8a**. A third stable hydrogen bond was observed between the NH-group (carbamate moiety) of **8a** and the backbone oxygen atom of Gly407 (SI **Figure S12A**). In the complex ALOX15-**8a**(A)-LA(B) the LA molecule is stretched out in the putative substrate binding pocket of conformer B (**Figure 5A**). Its carboxylate group interacted with the enzyme protein *via* two hydrogen bonds to two Arg side chains: i) Arg403, ii) Arg599. Both interactions were maintained during the entire MD simulation period. The methyl tail of LA is located close to the bottom of the substrate binding cavity that is formed by Ile418, Met419 and Ile593 as suggested by the Triad Concept[46]. The presence of the inhibitor **8b** in substrate binding pocket of conformer A (ALOX15-**8b**(A)-LA(B) complex) (SI **Figure S12B**) modifies the shape of the substrate binding cavity of conformer B (SI **Figure S12D**). Now, the two Arg residues (Arg403, Arg599) that anchor the carboxylic group of the substrate fatty acid, are blocked in this complex. Consequently, the mode of LA binding is altered and the substrates carboxylate forms new hydrogen bonds with Arg405 and Asn152. The tail of linoleic acid remains in a similar position regardless whether **8a** or **8b** was present in the cavity of conformer A. For better visualization of the global differences between ALOX15-**8a**(A)-LA(B) and ALOX15-**8b**(A)-LA(B) complexes the cavity surfaces of conformer B for both complexes are shown in **Figure 5C-D**.

Finally, we performed docking studies to define the most favourable binding mode for AA in the pocket of conformer B in the ALOX15-**8a**(A)-AA(B) and ALOX15-**8b**(A)-AA(B) complexes. Here again, the best AA poses were taken as the initial structures for MD simulations of both systems. Along the MD trajectory of the ALOX15-**8a**(A)-AA(B) complex we found that **8a** adopts a different conformation when compared with its shape in ALOX15-**8a**(A)-LA(B) MD simulation. Thus, inhibitor **8a** may be present in two different poses in the conformer A depending on the chemistry of the substrate (AA *vs.* LA) that is present at the active site of conformer B. The structure of the enzyme-inhibitor-complex appears to be more rigid when **8b** is bound in the putative substrate binding pocket of conformer A. In fact, this inhibitor presents the same binding mode in the three complexes studied here [ALOX15-**8b**(A)-empty(B) (see SI), ALOX15-**8b**(A)-LA(B), ALOX15-**8b**(A)-AA(B)]. The AA's carboxylate group interacts with Arg599 *via* two hydrogen bonds (**Figure 5B**) and both interactions are maintained during the whole MD simulation period. The tail of AA moves along the trajectory but remains at the bottom of the cavity surrounded by residues Ile418, Met419 and Ile593 as suggested by the Triad

Table 2. Average distances of C_{11} (and its hydrogen atoms) of LA to the OH-group for the system without inhibitor, with inhibitor 8a and inhibitor 8b along with the percentage of well-oriented structures

System	d(C_{11}-OH) (Å)	d(H_{11proS}-OH) (Å)	d(H_{11proR}-OH) (Å)	Well-oriented structures (%)
No inhibitor*	4.6	4.7	4.6	90.09
8a**	5.6	5.8	5.6	78.89
8b	5.5	6.2	5.6	34.00

*These results correspond to the MD simulation of the ALOX15-LA(B) complex. **In the ALOX15-8a(A)-LA(B) system the averages were calculated over the second 100ns-period of the MD trajectory.

Table 3. Average distances of C_{13} (and its hydrogen atoms) of AA to the OH-group for the system without inhibitor, with inhibitor 8a and inhibitor 8b along with the percentage of well-oriented structures

System	d(C_{13}-OH) (Å)	d(H_{13proS}-OH) (Å)	d(H_{13proR}-OH) (Å)	Well-oriented structures (%)
No inhibitor*	5.2	4.8	5.5	97.78
8a	5.4	4.9	6.0	88.47
8b	6.4	6.0	7.0	87.90

*These results correspond to the MD simulation of the ALOX15-AA(B) complex.

Concept[46]. In contrast, in the ALOX15-**8b**(A)-AA(B) complex the presence of inhibitor **8b** in the conformer A modifies the shape of the cavity of conformer B. Arg403 and Arg599 are blocked in this complex. Although the binding mode of AA changes somewhat with respect to its head (new hydrogen bonds are formed between AA carboxylate group and Arg405, Asn152, and Lys146), the tail of the substrate fatty acid remains at the same region as observed for ALOX15-**8a**(A)-AA(B) complex. Thus, in the ALOX15-**8a**(A)-LA(B) and the ALOX15-**8b**(A)-LA(B) complexes the substrate molecules adopt different conformations. These differences are related to the number of well-oriented structures found in both cases (**Table 2**). When **8b** is present in the system it causes a clear reduction of the well-oriented LA structures (those structures with the C11-H bond well-oriented for the H-abstraction) in comparison to the number of well-oriented structures obtained for **8a** system. In the ALOX15-**8a**(A)-LA(B) simulation we have found 79% of well-oriented structures for the H11-abstraction reaction from the total number of selected snapshots, whereas there is only 34% in the case of the ALOX15-**8b**(A)-LA(B) system (**Table 2,** SI **Figure S10**). This data indicates that LA is bound to ALOX15 in a less reactive conformation with respect to the orientation of the hydrogen atoms attached to C11. For AA the situation is somewhat different. With this substrate the number of well-oriented structures at C13 (the structures with the C13-H bond well-oriented for the H-abstraction) in the system appears to be similar for both, the ALOX15-**8a**(A)-AA(B) (88.5%) and the ALOX15-**8b**(A)-AA(B) (88%) complexes (**Table 3,** SI **Figure S11**).

DISCUSSION

Mammalian ALOX15 are allosteric enzymes and the substrate specificity and kinetic parameters of oxygenation are affected by their own products, 13-H(p)ODE and 12- and 15-H(p)ETE, formed from LA and AA, respectively[33-34]. Although the existence of allosteric sites that bind endogenous ALOX products[47] or other molecules[48-50] have previously been suggested there is no direct structural data supporting this hypothesis. As COX2 that forms stable catalytically active dimers in aqueous solutions, in which one monomer may function as allosteric regulator whereas the other monomer is catalytically active[51], rabbit ALOX15 might also form dimers. However, in contrast to COX2 and humanALOX5[52] or ALOX12[31] these dimers (weak self-associates) may be formed in solution via transient geometrical interfaces of structurally different enzyme conformations.[31, 35] Moreover, there is a dynamic equilibrium between monomeric and dimeric fractions[31]. Under hypotonic conditions (20 mM Tris) the enzyme is mainly present as monomer, whereas, at physiological salt concentrations dimerization is favoured[31].

In the crystal structure of rabbit ALOX15 (PDB entry 2PoM) the enzyme is present as mixed dimer, in which two conformers A and B interact with each other *via* their α2 and α18 helices.[32] Mutagenesis studies combined with SAXS measurements in aqueous solution suggested the importance of integrity of the hydrophobic inter-monomer interface for ALOX15 stability and its catalytic properties. Numerous contacts between the two helices α2 and α18 restrain the mobility of the two monomers within the ALOX15 dimer. Mutagenesis studies suggested that rearrangements of inter- and intra-molecular contacts of helix 18 may correlate with the volume of the putative substrate binding cavity of the catalytic monomer in the ligand bound ALOX 15 dimer and, thus, may fine-tune the reaction specificity of the enzyme.[42] This hypothesis is consistent with a recent report that showed that dimerization of human ALOX12 affect the enzymatic activity of this enzyme *via* allosteric mechanism.[53]

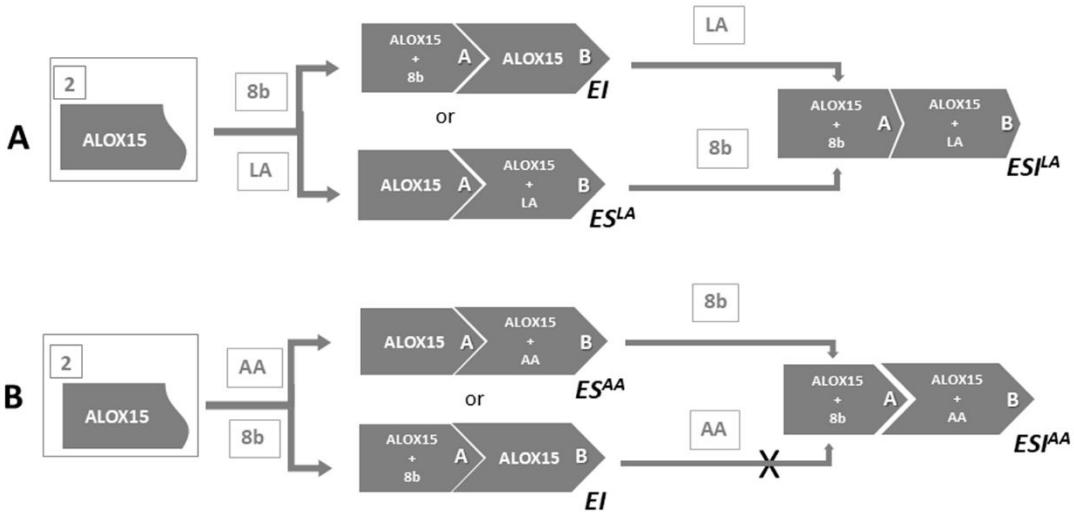

Figure 6. Schematic representation of the mechanism of proposed for action of **8b**.

Here we report that *N*-substituted 5-(1H-indol-2-yl)-2-methoxyanilines **6b, 6c**, **8b and 8c** may selectively inhibit linoleate oxygenase activity of rabbit and human ALOX15 with IC50-values in the lower two-digit nanomolar range without affecting the rate of AA oxygenation. Since ALOX15 exhibits comparable binding affinities for LA and AA[54-55] a conventional mode of inhibition predicts that oxygenation of the two substrates should be inhibited to a similar extent at a given inhibitor concentration. However, we observed remarkable substrate-specific ALOX15 inhibition by **8b** or **6c** and this substrate specificity can best be explained by an allosteric enzyme-inhibitor interaction. Extensive kinetic measurement suggested that inhibition of LA oxygenation by **8b** or **6c** may be best described by a non-competitive inhibition model. Here the substrate affinity (K_M) remains constant, but k_{cat} goes down (**Figure 3A,C**). This data suggests that binding of LA as oxygenation substrate and binding of the inhibitor are independent processes, but that the ternary complex (ESI^{LA}) may not be productive. In contrast, for AA the best fit of the experimental data suggested an uncompetitive mode of inhibition. In this case K_M and k_{cat} were reduced to similar extents (SI **Figures S5 and S6**) at increasing inhibitor concentrations. A reduction of the K_M-value suggests a better enzyme-substrate binding owing to constant depletion of the ES^{AA} complex upon inhibitor binding (ESI^{AA} formation). These data suggest that the inhibitor can preferentially bind to the enzyme-substrate complex (ES^{AA}), forming a non-productive ternary complex (ESI^{AA}). Here, one might suggest that when LA binds to ALOX15 or when its product (13-H(p)ODE) is formed during lipoxygenase reaction the ES^{LA} complex is formed (**Figure 6A**). The later binds **8b** to form the non-productive ESI^{LA} complex. On the other hand, it might be possible that **8b** binds first to form the dimeric ALOX15-**8b**(A)-empty(B) complex EI (**Figure 6A**) and this scenario will resemble the situation observed in the crystal structure (2PoM). In fact, our MD simulations supported the rigidity and stability of such a complex (see supporting information, SI **Figure S12**). When EI is formed, no AA binding may be possible any more owing to conformational restrictions (**Figure 6B**). Which of these mechanistic scenarios may correctly reflect the experimental data will be studied in a follow-up paper.

When no OCH_3-group was present at the aniline moiety of the core pharmacophore (compound **8a**) no substrate selectivity in enzyme inhibition was observed. The experimental data for **8a** were best fitted to a mixed model of inhibition and analysis of the experimental data (SI **Figure S7**) suggest that **8a** may compete with both AA and LA for binding at the active site of the enzyme (**Figure 3E,F**). Our MD simulations indicated that rigid location of **8b** in the putative substrate binding pocket of one monomer may fix the structure of the binding cavity of another monomer in dimer. In turn, **8a** adopts different positions depending on the chemistry of the substrate (AA *vs.* LA). Thus, **8a** that is not bounded as tightly when compared with **8b,** does not cause this structural modification. In the presence of **8b** LA is bound at the substrate binding pocket of the catalytic monomer in a less productive conformation. In contrast, for AA the number of well-oriented substrate structures (those structures in which the C13-H bond are well-oriented for the H-abstraction) is not affected by the inhibitor (**Tables 2 and 3**).

Human and rabbit ALOX15 orthologs exhibit dual positional specificity as they form both 15- and 12-hydroperoxides during AA oxygenation.[56-57] In fact, a 15- to 12-H(p)ETE ratio of 95.3±0.2 *vs.* 4.7±0.2 and 90.2±0.6 vs. 9.8±0.8 were previously reported for recombinant rabbit and human ALOX15, respectively.[42] Here we found that that neither **8a** nor **8b** impacted the product specificity of the rabbit enzyme with AA, but the product specificity of human enzyme was slightly altered (SI **Figure S9**). In other words, in the presence of **8a** or **8b** the human enzyme allows AA to adopt different conformation in the substrate binding pocket, which slightly favours AA 12-

lipoxygenation. Human and rabbit ALOX15 orthologs share an amino acid identity of 71 % and, thus, there are structural differences between the two enzymes. These differences might be responsible for these observations. Although the structural basis for this subtle difference has not been explored in detail it might be possible that inhibitor **8b** binding at one monomer of the ALOX15 dimer may induce minor structural alterations in the geometry of the catalytic cavity of the other monomer and, hence, might impact the alignment of the substrate fatty acid at the active site.

Additional evidence for the proposed allosteric mechanism of **8b** induced substrate-specific ALOX15 inhibition was provided by mutagenesis studies. When we explored the inhibition behaviour of the Leu183Glu+L192Glu double mutant of rabbit ALOX15, for which disruption of the inter-monomer interface within the ALOX15 dimer (PDB ID 2PoM) has previously been reported,[44] we found that these mutations prevented the substrate specific inhibition of the LA oxygenase activity by **8b** (**Figure 4**). For the mutant enzyme, the IC_{50} values obtained for LA and AA oxygenation were very similar. Although the IC_{50}-values of **8a** and **8b** obtained for the enzyme mutant were higher than those for the wild-type enzyme, there was no pronounced substrate specific inhibition.

In this study we observed that **8b** selectively inhibited linoleate oxygenase activity of human and rabbit ALOX15. Interestingly, no difference in the degree of inhibition of LA and AA was detected when mouse ALOX15 was used as catalyst. Although human ALOX15 shares about 74% of amino acid identity with its mouse ortholog, the murine enzyme lacks Gln596 that is conserved in the ALOX15 orthologs of rabbits, men and other higher primates. Recently, this residue has been reported to contribute to the allosteric properties of rabbit ALOX15[42]. In contrast, in rodents (rat, mouse) a Leu is present at position 596 but it remains unclear whether this amino acid exchange may affect the allosteric property of the enzyme.

There are reports in the literature suggesting that ALOX15 monomers involve allosteric binding sites[48-49] but for the time being such binding sites have not convincingly been characterized. On the other hand, the results obtained in this study are consistent with the formation of non-covalently linked dimeric enzyme associates in aqueous solutions. Although sedimentation velocity analytical ultracentrifugation established the gold standard in aggregation analytics[58-59], it cannot be applied to study reversible ALOX15 dimerization in diluted protein solutions. This method requires protein amounts that are at least 100-fold higher than those used in our kinetic assays (2-4 µg/ml). Unfortunately, for the time being, there is no direct experimental proof for either of these two possible explanations.

CONCLUSIONS

Here we describe the chemical synthesis and functional characterization of novel substrate-specific ALOX15 inhibitors and suggest an allosteric model for their inhibitory activity. This model is based on our previous observations that ALOX15 may form transient dimers in aqueous solutions so that inhibitor binding at the substrate binding pocket of one monomer may induce conformational changes in the catalytic cavity of the other monomer. The 2-methoxyaniline moiety attached to the core pharmacophore appears to be crucial for the substrate selectivity of ALOX15 inhibition.

EXPERIMENTAL SECTION

Chemistry. The solvent and reagents were purchased from Acros or Sigma-Aldrich (Schnelldorf, Germany) and were used without further purification unless otherwise noted. ^{1}H and ^{13}C NMR spectra were recorded with a 300 MHz Brucker MSL spectrometer in $CDCl_3$ or acetone-d_6 using tetramethylsilane as the internal standard for ^{1}H-NMR. Chemical shifts in ^{13}C-NMR were referenced to the residual carbon signal of $CDCl_3$ and acetone-d_6 at δ ^{13}C = 77.19 and 206.26 ppm, respectively. Chemical shifts are given in ppm, spin-spin interaction constants in Hz. IR spectra were recorded using a Brucker Equinox 55 spectrometer (Germany) at 4 cm^{-1} resolution. Elemental analysis was performed with a Thermo Finnigan FLASH EA 1112 analyzer (Italy). Flash column chromatography was carried out using silica gel (Acros, Germany, particle size 60-200 µm) as stationary phase. Silica gel 60 F^{254} plates (Merck, Germany) were used for thin-layer chromatography (TLC). Spots were detected under UV light or after staining with an ethanolic (3%) solution of vanillin. Analytical HPLC of all compounds was performed on a Shimadzu LC-10Avp liquid chromatograph equipped with a SPD-10Advp UV detector (Japan) using a Nucleodur C18 Gravity column (Macherey-Nagel, Düren, Germany; 250 x 4 mm, 5 µm particle size) coupled with a guard column (8 x 4 mm, 5 µm particle size) at a flow rate of 1 mL/min. For compounds **5a**-**5c** the solvent system consisted of a mixture of acetonitrile : 10 M ammonium formate (50:50, v/v) and its pH was adjusted to pH 3.0 with formic acid. For all other compounds we used acetonitrile : water : acetic acid (70:30:0.1, v/v). Preparative HPLC was performed using a Knauer HPLC pump 64 system coupled with a differential refractometer and UV-VIS detector (Knauer, Germany). A Luna C18(2) column (75 × 30.0 mm, particle size 5 µm, Phenomenex, USA) and isocratic systems of different compositions of solvents A and B at a flow rate of 25 mL / min were applied to achieve the best chromatographic performance. Solvent A was HPLC-grade acetonitrile. A polar component of the system (solvent B) was a 10 M solution of ammonium formate adjusted with formic acid to pH 3.0. All compounds were >95% as indicated by analytical HPLC. Mass spectra (EI) were recorded on an Agilent a 6890N gas chromatograph coupled with 5973N mass spectral detector (Agilent, USA) using a DB-5ms column (30 m, coating thickness 0.5 µm, Agilent J&W, USA). An injector temperature of 250 °C, an ion source temperature of 230 °C and the electron energy of 70 eV were set. Helium was used as carrier gas at a flow rate of 1.0 mL / min. Samples were eluted using the

following temperature program: isothermally at 70 °C for 5 min, then from 70 to 290 °C at a rate of 30 °C/min, followed by isothermal step at 290°C for 10 min. Finally, the column was conditioned at 310 °C for 30 min. HRMS were obtained on the Bruker micrOTOF II mass spectrometer with an electrospray ionization (ESI). The measurements were performed using either positive or negative ionization mode. Interface capillary voltage was set up at 4500 V and the mass range from m/z 50 to 3000 Da. External or internal calibration was performed with Electrospray Calibration Solution (Fluka). N_2 was applied as a drying gas.

*1-(4-methoxy-3-aminophenyl)ethanone (**2**).* To an ethanolic solution (100 mL) of 1-(4-methoxy-3-nitrophenyl) ethanone 1 (11.1 g, 56.92 mmol) 0.55 g (5 % m/m) of 10% Pd/C-catalyst and ammonium formate (10.8 g, 171.26 mmol) were added. The resulting mixture was kept for 3 h under reflux. After the reduction was complete the catalyst was filtered off, the solvent was evaporated under reduced pressure and the dry residue was dissolved in 50 mL of saturated K_2CO_3 solution. The organic products were extracted with CH_2Cl_2 (4 x 20 mL), the combined organic extracts were dried over Na_2SO_4 and concentrated. The raw product was chromatographed using gradient elution with EtOAc/Pet (from 25 to 50% EtOAc) to yield 8.5 g (90.5%) of compound **2**. R_f = 0.66 (EtOAc/Pet 1: 1). IR (KBr): ν 3446 cm^{-1} (s), 3354 cm^{-1} (s). ^{1}H NMR (300 MHz, $CDCl_3$) δ 7.35 (d, J = 8.32, 2.12 Hz, 1H), 7.31 (d, J = 2.13 Hz, 1H), 3.88 (s, 3H), 2.49 (s, 3H). ^{13}C NMR (75 MHz, $CDCl_3$) δ = 197.34, 151.29, 136.31, 130.75, 120.44, 113.99, 109.31, 55.67, 26.28. Elemental analysis calcd: C 65.44, H 6.71, N 8.48, found: C 65.34, H 6.77, N 8.54. MS (70 eV): m/z (%): 150 (100), 165 (84), 122 (29).

*General method for preparation of hydrazones **4a-c**.* A solution of phenylhydrazine **3a-b** (1.20 mmol) and ethanone **2a-b** (0.6 mmol) in 6 mL of a mixture of ethanol-acetic acid (5: 1, v/v) was refluxed for 18 h. After the reaction mixture was cooled down it was stirred at room temperature for one additional hour. The precipitated hydrazones **4a-b** were filtered off, washed with hexane (10 mL), dried and used for further synthesis without additional purification.

*General procedure for the preparation of aminoarylindoles **5a-c**.* Method A: A mixture of the hydrazone **4a-c** (1.89 mmol) and ZnCl2 (15.13 mmol) was heated to 180 °C for 2 h. The reaction mixture was then cooled down and quenched with 10% HCl (50 mL). The precipitate was filtered off, the filtrate was alkalized with 25% aqueous ammonia until a pH 13 was reached and extracted with CH_2Cl_2 (3 x 25 mL). The combined organic extracts were evaporated under reduced pressure. The raw product was chromatographed on silica gel using gradient elution with THF/Pet (from 20 to 66% THF). The yields of the aminoarylindoles **5a-c** were only 5-10%. Method B: A mixture of 80% polyphosphoric acid (2.07 mmol), phenylhydrazine **3a-b** (1.38 mmol) and ethanone **2a-b** (1.38 mol) was heated to 130 °C and kept at this temperature for 30 minutes. After the reaction mixture was cooled down, it was quenched with water (100 mL) and alkalized with 25% aqueous solution of ammonia until pH 13 was reached. The precipitate was filtered off and recrystallized from a mixture ethanol/water (1:1, v/v). The raw product that remained in the mother liquor was chromatographed on silica gel using gradient elution with THF/Pet (from 20 to 66% THF).

*3-(1H-indol-2-yl)aniline (**5a**):* Yield by method B: 60%. m.p.: 168 °C (lit. 166 °C)[38]. R_f = 0.53 (EtOAc / Pet 1: 1, v/v). Analytical RP-HPLC: R_t 11.27 min (235 and 310 nm). IR (KBr): ν 3440 cm^{-1} (s), 3399 cm^{-1} (s), 1611 cm^{-1} (s). UV/Vis λ_{max} 228 nm, 310 nm. ^{1}H NMR (300 MHz, acetone-d_6) δ 10.48 (s, 1H), 7.53 (dm, J = 7.76 Hz, 1H), 7.39 (dq, J = 8.06, 0.88 Hz, 1H), 7.16 - 6.97 (m, 5H), 6.76 (dd, J = 2.26, 0.92 Hz, 1H), 6.64 (ddd, J = 7.49, 2.28, 1.50 Hz, 1H), 4.66 (s, 2H). ^{13}C NMR (75 MHz, acetone-d_6) δ 149.75, 139.74, 138.24, 134.33, 130.33, 122.28, 120.90, 120.28, 114.77, 114.70, 111.95, 99.38. MS (70 eV) m/z (%): 208.1 (100), 180 (18). Elemental analysis calcd: C 80.74, H 5.81, N 13.45; found: C 80.68, H 5.73, N 13.36.

*5-(1H-indol-2-yl)-2-methoxyaniline (**5b**):* Yield by method B: 52%. m.p.: 208.2 °C (lit. 208-209 °C).[27] R_f = 0.41 (EtOAc / Pet 1: 1, v/v). Analytical RP-HPLC: R_t 11.42 min (235 and 310 nm). IR (KBr): ν 3440 cm^{-1} (s), 3399 cm^{-1} (s), 1611 cm^{-1} (s), 1449 cm^{-1} (m). UV/Vis λ_{max} 230 nm, 312 nm. ^{1}H NMR (300 MHz, acetone-d_6) δ 10.49 (s, 1H), 7.50 (dm, J = 7.73 Hz, 1H), 7.36 (dm, J = 7.96 Hz, 1H), 7.20 (d, J = 2.23 Hz, 1H), 7.12 - 6.97 (m, 3H), 6.88 (d, J = 8.35 Hz, 1H), 6.66 - 6.65 (m, 1H), 4.50 (s, 2H), 3.85 (s, 3H). ^{13}C NMR (75 MHz, acetone-d_6) δ 147.80, 139.91, 138.77, 138.10, 130.43, 126.64, 121.83, 120.58, 120.15, 114.92, 111.99, 111.73, 111.44, 98.25, 55.89. MS (70 eV) m/z (%): 223 (100), 238 (75). Elemental analysis calcd: C 74.61, H 5.92, N 11.76; found: C 74.57, H 5.91, N 11.69.

*5-(5-fluoro-1H-indol-2-yl) -2-methoxyaniline (**5c**):* Yield by method B: 58%. m.p.: 221-223 °C. R_f = 0.45 (CH_2Cl_2 with 5% NH_3). Analytical RP-HPLC: R_t = 11.82 min (235 and 310 nm). IR (KBr): ν 3439 cm^{-1} (m), 3351 cm^{-1} (m), 3291 cm^{-1} (m) 1611cm^{-1} (s), 1449 cm^{-1} (vs), 1186 cm^{-1} (m). UV/Vis λ_{max} 228 nm, 322 nm. ^{1}H NMR (300 MHz, acetone-d_6) δ 10.58 (s, 1H), 7.34 (ddt, J = 8.76, 4.58, 0.73 Hz, 1H), 7.22 - 7.17 (m, 2H), 7.09 (dd, J = 8.29, 2.20 Hz, 1H), 6.88 (d, J = 8.33 Hz, 1H), 6.86 – 6.80 (m, 1H), 6.66 - 6.65 (m, 1H), 4.52 (s, 2H), 3.86 (s, 3H). ^{13}C NMR (75 MHz, acetone-d_6) δ 160.24, 157.17, 147.99, 141.95, 138.83, 134.65, 130.79, 130.66, 126.19, 115.00, 112.54, 112.41, 111.95, 111.39, 109.79, 109.44, 105.18, 104.87, 98.44, 98.38, 55.87. MS (70 eV) m/z (%): 241 (100), 256 (75). Elemental analysis calcd: C 70.30, H 5.11, N 10.93; found: C 69.51, H 5.29, N 10.66.

*General procedure for the preparation of substituted 2-arylindolesulfocarbomats **6a-c–8a-c**.* To a solution of chlorosulfonyl isocyanate (0.27 mmol) and the corresponding alcohol (0.25 mol) in 3 mL of dry CH_2Cl_2 Et_3N (0.38 mmol) was added and the mixture was stirred for 15 min at rt. After that a solution of arylindole **5a-e** (1.0 mol) in 3 mL of dry CH_2Cl_2 was added to the mixture and the reaction was left overnight at room temperature. After the reaction was complete, it was quenched with water (10 mL). The organic layer was separated and dried with Na_2SO_4, concentrated under reduced pressure and the raw

product was purified on silica gel using a gradient elution with THF/Pet (from 20 to 66% THF) followed by preparative RP-HPLC (solvent A/ solvent B 60:40 or 65:35, v/v, 235 or 310 nm) for all compounds.

*Isobutyl (N-(3-(1H-indol-2-yl)phenyl)sulfamoyl)carbamate (**6a**):* Yield: 29.9%. R_f = 0.4 (THF / Pet 1: 1, v/v). Analytical RP-HPLC: R_t 4.64 min (235 and 320 nm), purity 99.0%. UV/Vis λ_{max} 233 nm, 309 nm. ^{1}H NMR (300 MHz, acetone-d_6) δ = 10.66 (s, 1H), 7.82 (t, J = 1.73 Hz, 1H), 7.65 (ddd, J = 7.79, 1.74, 1.02 Hz, 1H), 7.58 (dm, J = 7.88 Hz, 1H), 7.45 - 7.40 (m, 2H), 7.25 (ddd, J = 8.04, 2.20, 1.01 Hz, 1H), 7.12 (ddd, J = 8.17, 7.05, 1.26 Hz, 1H), 7.03 (ddd, J = 8.05, 7.09, 1.12 Hz, 1H), 6.87 (dd, J = 2.25, 0.92 Hz, 1H), 3.88 (d, J = 6.64 Hz, 2H), 1.85 (hept, J = 13.37, 6.74 Hz, 1H), 0.81 (d, J = 6.73 Hz, 6H). ^{13}C NMR (75 MHz, acetone-d_6) δ 152.31, 139.10, 138.58, 138.33, 134.87, 130.66, 130.15, 122.94, 122.33, 121.23, 120.67, 120.64, 118.28, 112.19, 100.58, 72.67, 28.58, 18.97. HRMS (ESI): calculated for $[M+H]^+$ = 388.1326, found $[M+H]^+$ = 388.1330 (50.6 %), error ppm = 1.030575633; calculated for $[M+Na]^+$ = 410.1145, found $[M+Na]^+$ = 410.1154 (100 %), error ppm = 2.194509094.

*Isobutyl (N-(3-(1H-indol-2-yl)methoxyphenyl)sulfamoyl)-carbamate (**6b**):* Yield: 55.7%. R_f = 0.31 (THF / Pet 1: 1, v/v). Analytical RP-HPLC: R_t 5.43 min (235 and 320 nm), purity 99.5%. UV/Vis λ_{max} 225 nm, 311 nm. ^{1}H NMR (300 MHz, acetone-d_6) δ 7.92 (d, J = 1.93 Hz, 1H), 7.63 (dd, J = 8.53, 2.23 Hz, 1H), 7.54 (ddd, J = 7.71, 1.33, 0.79 Hz, 1H), 7.40 (dm, J = 10.05 Hz, 1H), 7.15 (d, J = 8.57 Hz, 1H), 7.12 – 6.98 (m, 2H), 6.77 (d, J = 0.91 Hz, 1H), 3.90 (d, J = 6.61 Hz, 2H), 1.87 (hept, J = 6.71 Hz, 1H), 0.85 (d, J = 6.74 Hz, 6H). ^{13}C NMR (75 MHz, acetone-d_6) δ 152.07, 150.51, 138.36, 138.19, 130.23, 127.42, 126.76, 123.10, 122.42, 120.87, 120.46, 118.64, 112.68, 111.90, 99.33, 72.69, 56.69, 28.53, 18.97. HRMS (ESI): calculated for $[M+H]^+$ = 418.1430, found $[M+H]^+$ = 418.1426 (81.2 %), error ppm = 0.956610537; calculated for $[M+Na]^+$ = 440.1250, found $[M+Na]^+$ = 440.1242 (100 %), error ppm = 1.817665436; calculated for $[M+K]^+$ = 456.0990, found $[M+K]^+$ = 456.0980 (40.4 %), error ppm = 2.192506451.

*Isobutyl (N-(5-(5-fluoro-1H-indol-2-yl)-2-methoxyphenyl)-sulfamoyl)carbamate (**6c**):* Yield: 63.1%. R_f = 0.21 (THF / Pet 1: 1, v/v). Analytical RP-HPLC: R_t 5.55 min (235 and 320 nm), purity 98.5%. UV/Vis λ_{max} 224 nm, 315 nm. ^{1}H NMR (300 MHz, acetone-d_6) δ 10.72 (s, 1H), 7.92 (d, J = 2.24 Hz, 1H), 7.62 (dd, J = 8.57, 2.28 Hz, 1H), 7.39 (dd, J = 8.77, 4.50 Hz, 1H), 7.24 (dd, J = 9.86, 2.55 Hz, 1H), 7.16 (d, J = 8.56 Hz, 1H), 6.87 (td, J = 9.16, 2.56 Hz, 1H), 6.76 (s, 1H), 3.94 (s, 3H), 3.89 (d, J = 6.58 Hz, 2H), 1.87 (hept, J = 13.43, 6.70 Hz, 1H), 0.85 (d, J = 6.73 Hz, 6H). ^{13}C NMR (75 MHz, acetone-d_6) δ 160.37, 157.30, 152.25, 150.73, 140.41, 134.78, 130.63, 130.49, 127.57, 126.36, 123.20, 118.68, 112.81, 112.70, 110.50, 110.15, 105.46, 105.14, 99.48, 99.42, 72.68, 56.71, 28.54, 18.98. HRMS (ESI): calculated for $[M+H]^+$ = 436.1337, found $[M+H]^+$ = 436.1332 (100 %), error ppm = 1.146437434; calculated for $[M+Na]^+$ = 458.1156, found $[M+Na]^+$ = 458.1151 (46.9 %), error ppm = 1.091427579; calculated for $[M+K]^+$ = 474.0896, found $[M+K]^+$ = 474.0888 (2.0 %), error ppm = 1.687444736.

*Allyl (N-(3-(1H-indol-2-yl)phenyl)sulfamoyl)carbamate (**7a**):* Yield: 36.1% R_f = 0.57 (THF / Pet 1: 1). Analytical RP-HPLC: R_t 3.78 min (235 and 320 nm), purity 98.5%. UV/Vis λ_{max} 233 nm, 307 nm. ^{1}H NMR (300 MHz, acetone-d_6) δ = 7.83 (t, J = 1.98 Hz, 1H), 7.64 (dm J = 7.80 Hz, 1H), 7.58 (dm, J = 7.78 Hz, 1H), 7.47 – 7.38 (m, 2H), 7.26 (ddd, J = 8.05, 2.20, 1.05 Hz, 1H), 7.12 (ddd, J = 8.21, 7.02, 1.29 Hz, 1H), 7.03 (ddd, J = 8.08, 7.04, 1.12 Hz, 1H), 6.88 – 6.84 (m, 1H), 5.84 (ddt, J = 17.28, 10.64, 5.44 Hz, 1H), 5.21 (dq, J = 17.29, 1.61 Hz, 1H), 5.09 (dq, J = 10.58, 1.48 Hz, 1H), 4.57 (dt, J = 5.50, 1.51 Hz, 2H). ^{13}C NMR (75 MHz, acetone-d_6) δ 152.58, 139.15, 138.29, 138.10, 134.63, 132.97, 130.58, 129.95, 122.81, 122.06, 121.13, 120.51, 120.36, 118.27, 117.89, 112.10, 100.35, 66.90. HRMS (ESI): calculated for $[M+H]^+$ = 372.1013, found $[M+H]^+$ = 372.1004 (100 %), error ppm = 2.418696199; calculated for $[M+Na]^+$ = 394.0832, found $[M+Na]^+$ = 394.0824 (53.5 %), error ppm = 2.030028177; calculated for $[M+K]^+$ = 410.0571, found $[M+K]^+$ = 410.0562 (15.1 %), error ppm = 2.194816283.

*Allyl (N-(3-(1H-indol-2-yl)methoxyphenyl)sulfamoyl)carbamate (**7b**):* Yield: 49.9% R_f = 0.58 (THF / Pet 1: 1). Analytical RP-HPLC: R_t 4.29 min (235 and 320 nm), purity 98.0%. UV/Vis λ_{max} 225 nm, 311 nm. ^{1}H NMR (300 MHz, acetone-d_6) δ 7.92 (d, J = 2.24 Hz, 1H), 7.64 (dd, J = 8.56, 2.24 Hz, 1H), 7.55 (ddd, J = 7.71, 1.33, 0.79 Hz, 1H), 7.40 (dq, J = 8.07, 0.93 Hz, 1H), 7.15 (d, J = 8.59 Hz, 1H), 7.12 – 6.98 (m, 2H), 6.77 (d, J = 0.90 Hz, 1H), 5.89 (ddt, J = 17.26, 10.64, 5.43 Hz, 1H), 5.26 (dq, J = 17.26, 1.63 Hz, 1H'), 5.17 (dq, J = 10.52, 1.41 Hz, 1H''), 4.62 (dt, J = 5.41, 1.51 Hz, 2H). ^{13}C NMR (75 MHz, acetone-d_6) δ 151.91, 150.66, 138.35, 138.19, 132.94, 130.23, 127.40, 126.73, 123.17, 122.41, 120.87, 120.45, 118.92, 118.30, 112.72, 111.90, 99.32, 67.09, 56.69. HRMS (ESI): calculated for $[M+H]^+$ = 402.1118, found $[M+H]^+$ = 402.1113 (100 %), error ppm = 1.2434356283; calculated for $[M+Na]^+$ = 424.0938, found $[M+Na]^+$ = 424.0934 (48.7 %), error ppm = 0.943187568; calculated for $[M+K]^+$ = 440.0677, found $[M+K]^+$ = 440.0673 (4.2 %), error ppm = 0.908951055.

*Allyl (N-(5-(5-fluoro-1H-indol-2-yl)-2-methoxyphenyl)-sulfamoyl)carbamate (**7c**):* Yield: 52.3%. R_f = 0.32 (THF / Pet 2: 1, v/v). Analytical RP-HPLC: R_t 4.35 min (235 and 320 nm), purity 98.2%. UV/Vis λ_{max} 224 nm, 314 nm. ^{1}H NMR (300 MHz, acetone-d_6) δ 10.81 (s, 1H), 7.91 (d, J = 2.18 Hz, 1H), 7.64 (dd, J = 8.56, 2.20 Hz, 1H), 7.39 (dd, J = 8.76, 4.54 Hz, 1H), 7.25 (dd, J = 9.85, 2.57 Hz, 1H), 7.15 (d, J = 8.63 Hz, 1H), 6.89 (ddd, J = 9.59, 8.76, 2.54 Hz, 1H), 6.78 (dd, J = 2.22, 0.90 Hz, 1H), 5.88 (ddt, J = 17.19, 10.69, 5.41 Hz, 1H), 5.25 (dq, J = 17.24, 1.58 Hz, 1Ha), 5.17 (dq, J = 10.51, 1.40 Hz, 1Hb), 4.62 (dt, J = 5.41, 1.48 Hz, 2H), 3.92 (s, 3H). ^{13}C NMR (75 MHz, acetone-d_6) δ 160.41, 157.33, 151.78, 151.02, 140.50, 134.95, 132.88, 130.68, 130.55, 127.45, 126.42, 123.47, 119.15, 118.39, 112.87, 110.53, 110.18, 105.48, 105.16, 99.59, 99.52, 67.17, 56.74. HRMS (ESI): calculated for $[M+H]^+$ = 420.1024, found $[M+H]^+$ = 420.1037 (100 %), error ppm = 3.094483631; calculated for $[M+Na]^+$ = 442.0843, found $[M+Na]^+$ = 442.0856 (100 %), error ppm = 2.940615625; calculated for $[M+K]^+$ = 458.0583, found $[M+K]^+$ = 458.0591 (50 %), error ppm = 1.746502574.

*Octyl (N-(3-(1H-indol-2-yl)phenyl)sulfamoyl)carbamate (**8a**):* Yield: 38.6%. Rf = 0.53 (THF / Pet, 2:1, v/v). Analytical RP-HPLC: Rt 16.68 min (235 and 320 nm), purity 98.9%. UV/Vis λ_{max} 233 nm, 308 nm. ^{1}H NMR (300 MHz, acetone-d_6) δ 10.69 (s, 1H), 7.82 (t, J = 1.73 Hz, 1H), 7.65 (dm, J = 8.25 Hz, 1H), 7.57 (dm, J = 8.13 Hz, 1H), 7.45 – 7.40 (m, 2H), 7.25 (ddd, J = 8.03, 2.19, 1.02 Hz, 1H), 7.12 (ddd, J = 8.16, 7.05, 1.26 Hz, 1H), 7.03 (ddd, J = 8.18, 2.57, 1.25 Hz, 1H), 6.88 – 6.87 (m, 1H), 4.08 (t, J = 6.61 Hz, 2H), 1.56 – 1.52 (m, 2H), 1.31 – 1.15 (m, 10H), 0.84 (t, J = 6.84 Hz, 3H).^{13}C NMR (75 MHz, acetone-d6) δ = 152.35, 139.16, 138.56, 138.17, 134.80, 130.64, 130.11, 122.92, 122.20, 121.22, 120.61, 120.48, 118.04, 112.19, 100.52, 66.94, 32.59, 30.19, 29.95, 29.90, 26.34, 23.31, 14.34. HRMS (ESI): calculated for $[M-H]^+$ = 442.1806, found $[M-H]^+$ = 442.1819 (100 %), error ppm = 2.939975205.

*Octyl (N-(5-(1H-indol-2-yl)-2-methoxyphenyl)sulfamoyl)carbamate (**8b**):* Yield: 65.7%. R_f = 0,43 (THF / Pet 2: 1, v/v). Analytical RP-HPLC: R_t 15.16 min (235 and 320 nm), purity 98.5%. UV/Vis λ_{max} 226 nm, 312 nm. ^{1}H NMR (300 MHz, acetone-d_6) δ 11.05 (s, 1H), 8.10 (d, J = 2.21 Hz, 1H), 7.49 (dm, J = 7.68 Hz, 1H), 7.41 (dm, J = 7.97 Hz, 1H), 7.36 (dd, J = 8.42, 2.22 Hz, 1H), 7.05 – 6.93 (m, 2H), 6.86 (d, J = 8.50 Hz, 1H), 6.70 – 6.69 (m, 1H), 3.88 (t, J = 6.82 Hz, 2H), 3.88 (s, 3H), 1.52 – 1.43 (m, 2H), 1.28 – 1.15 (m, 10H), 0.83 (t, J = 6.76 Hz, 3H).^{13}C NMR (75 MHz, acetone-d_6) δ 161.23, 148.64, 139.80, 138.35, 131.78, 130.37, 126.47, 121.71, 120.50, 119.99, 119.25, 115.63, 112.08, 111.70, 98.37, 65.33, 56.31, 32.56, 30.15, 29.97, 29.94, 26.79, 23.27, 14.33. HRMS (ESI): calculated for $[M+H]^+$ = 474.2057, found $[M+H]^+$ = 474.2064 (100 %), error ppm = 1.476152649; calculated for $[M+Na]^+$ = 496.1877, found $[M+Na]^+$ = 496.1881 (100 %), error ppm = 0.806146545; calculated for $[M+K]^+$ = 512.1616, found $[M+K]^+$ = 512.1625 (50 %), error ppm = 1.757257865.

*Octyl (N-(5-(5-fluoro-1H-indol-2-yl)-2-methoxyphenyl)-sulfamoyl)carbamate (**8c**):* Yield: 62.5%. R_f = 0.15 (THF / Pet 2: 1, v/v). Analytical RP-HPLC: R_t 15.28 min (235 and 320 nm), purity 99%. UV/Vis λ_{max} 222 nm, 314 nm. ^{1}H NMR (300 MHz, acetone-d_6) δ 10.83 (s, 1H), 7.91 (d, J = 2.23 Hz, 1H), 7.63 (dd, J = 8.55, 2.24z Hz, 1H), 7.38 (dd, J = 8.87, 4.63 Hz, 1H), 7.24 (dd, J = 9.87, 2.53 Hz, 1H), 7.16 (d, J = 8.56 Hz, 1H), 6.87 (ddd, J = 9.59, 8.75, 2.52 Hz, 1H), 6.78 (dd, J = 2.27, 0.90 Hz, 1H), 4.09 (t, J = 6.59 Hz, 2H), 3.93 (s, 3H), 1.58 – 1.53 (m, 2H), 1.28 – 1.18 (m, 10H), 0.85 (t, J = 6.74 Hz, 3H).^{13}C NMR (75 MHz, acetone-d_6) δ 160.31, 157.24, 151.78, 150.64, 140.49, 134.87, 130.60, 130.46, 127.62, 126.30, 123.03, 118.48, 112.83, 112.70, 112.63, 110.44, 110.09, 105.41, 105.10, 99.44, 99.38, 66.94, 56.65, 32.48, 29.88, 29.84, 29.26, 26.32, 23.25, 14.32. HRMS (ESI): calculated for $[M+H]^+$ = 492.1963, found $[M+H]^+$ = 492.1960 (35.5 %), error ppm = 0.609512912; calculated for $[M+Na]^+$ = 514.1782, found $[M+Na]^+$ = 514.1773 (100 %), error ppm = 1.750365924; calculated for $[M+K]^+$ = 530.1522, found $[M+K]^+$ = 530.1523 (22.4 %), error ppm = 0.188625078.

Biochemistry general. The chemicals used were obtained from the following sources: arachidonic acid (5Z,8Z,11Z,14Z-eicosatetraenoic acid), 13(*S*)-HpODE,13(*S*)-HODE and HPLC standards of 15(*S*)-HETE and 12(S)-HETE from Cayman Chem (distributed by Biomol, Hamburg, Germany), HPLC grade methanol, acetonitril and acetic acid from Fisher Scientific (Nidderau, Germany), isopropyl-β-d-thiogalactopyranoside (IPTG) from Carl Roth GmbH (Karlsruhe, Germany). The E. coli strain XL-1 blue was purchased from Stratagene (La Jolla, CA), the Rosetta 2 strain BL21(DE3)pLysS were purchased from Invitrogen (Carlsbad, California, USA).

Preparation of rabbit ALOX15. Wild-type rabbit ALOX15 and several enzyme mutants were expressed as N-terminal His-tag fusion proteins in E. coli using the pQE-9 prokaryotic expression plasmid and XL-1 blue competent cells according to the protocol described previously.[60-61]

Preparation of human ALOX15. Human ALOX15 used in this study was expressed as N-terminal his-tag fusion proteins employing the E. coli strain Rosetta2(DE3)pLysS as overexpression system. Competent bacteria were transformed with 100 ng of the recombinant pET28b expression plasmid and the cells were grown overnight on kanamycin/chloramphenicol containing agar plates. An isolated clone was selected and two 1 mL bacterial liquid cultures (LB medium with 50 µg/mL kanamycin/35 µg/mL chloramphenicol) were grown at 37 °C and 180 rpm agitation for 6 h. Aliquots of these pre-cultures were added to a 50 to 500 mL main culture to reach an optical density (A600) of 0.10-0.15. Bacterial expression was carried out in 50 or 500 mL Ultra Yield culture flasks (Thomson Instrument Company, Oceanside, USA) using the optimized Enpresso-Expression system (Enpresso GmbH, Berlin, Germany) following the instructions of the vendor. After overnight incubation at 30°C and 250 rpm agitation, the OD600 had reached values above 5 and expression of the recombinant his-tag fusion proteins was induced by the addition of 1 mM (final concentration) IPTG. Then the cultures were maintained at 22 °C for 24 h at 230-250 rpm agitation. Bacteria were harvested, the resulting pellet was reconstituted in a total volume of 5 to 30 mL PBS and bacteria were disrupted at 15,000 psi with an Emulsiflex-C5 high-pressure cell homogenizer (Avestin, Ottawa, Canada). After the debris was removed by centrifugation (30 min, 14,000 g), the lysis supernatant was passed through a Ni-NTA column (Qiagen, Hilden, Germany) for purification (gel bed volume of 1.8 mL). The column was washed twice with 2 mL of washing buffer W1 (100mM Tris, pH 8.0, 200 mM NaCl, 10 mM imidazol), twice with 2 mL with washing buffer W2 (100 mM Tris, pH 8.0, 200 mM NaCl, 25 mM imidazol) and the adherent proteins were eluted 5 times with 0.6 ml of elution buffer (100mM Tris, pH 8.0, 200 mM NaCl, 200 mM imidazol). Enzyme containing fractions (E3-E5) were combined, supplemented with glycerol (10% final concentration), shock frozen in liquid nitrogen and stored at –80°C. After thawing the pooled Ni-NTA fractions were desalted on an Econo-Pac 10DG column (Bio Rad, Munich, Germany) and the recombinant proteins were further purified by FPLC on a Resource Q column (GE Healthcare Bio-Sciences AB, Uppsala, Sweden) as described previously for rabbit ALOX15[60-61]. The fractions that contained active protein were pooled together and used as final enzyme preparations.

Preparation of mouse ALOX. Recombinant mouse Alox15 (mAlox15), human Alox12 (hALOX12), mouse Alox12 (mAlox12), human ALOX15B and mouse Alox15b were expressed as N-terminal his-tag fusion proteins in employing the E. coli strain Rosetta2(DE3)pLysS strain as overexpression system. Competent bacteria were transformed with 50 ng of the recombinant pET28b expression plasmid and the cells were grown overnight on agar plates containing antibiotics. A well-isolated bacterial clone was picked using a wooden sterile toothpick and two 1 mL liquid cultures (LB medium with 50 µg/mL kanamycin/35 µg/mL chloramphenicol) were grown for 7 hours at 37° C. Aliquots of these pre-culture were added to a 50 mL main culture to reach an optical density (A600) of 0.10-0.15. Bacterial expression was carried out in 50 mL Ultra Yield culture flasks (Thomson Instrument Company, Oceanside, USA) using the optimized Enpresso-Expression system (Enpresso GmbH, Berlin, Germany). After overnight incubation at 30°C the OD600 had reached values above 5 and expression of the recombinant his-tag fusion proteins was induced by the addition of IPTG reraching a final concentration of 1 mM. Then the cultures were kept at 22 °C for 24 h at 230-250 rpm agitation. Bacteria were harvested, the resulting pellet was reconstituted in a total volume of 5 mL PBS and bacteria were lyzed by sonication using a digital sonifier (W-250D Microtip Model 102, 50% maximal sonication amplitude; Branson Ultraschall, Fürth, Germany). Cell debris was spun down (15 min, 15,000 x g, 4°C) and the lysate supernatants were employed as enzymes source for the inhibitor studies without further purification.

ALOX Activity Assay (purified enzymes). The oxygenation kinetics of linoleic acid [LA] or arachidonic acid [AA] (25 µM final concentrations) were assayed spectrophotometrically measuring the increase in absorbance at 235 nm. The assay mixture was a 0.1 M phosphate buffer, pH 7.4 containing various concentrations of inhibitors. For this purpose, compounds tested were reconstituted in DMSO and serial dilutions were carried out so that from each dilution 1 µL was applied for the measurement. Purified rabbitALOX15 [5 µg, specific activity with LA - 25 s^{-1}, electrophoretical purity (>98%)] or human ALOX15 [5 µg, specific activity with LA - 10 s^{-1}, electrophoretical purity (>98%)] were pre incubated with a testing compound for 1 min and the reaction was started by the addition of the substrate. The linear part of the kinetic progress curve was evaluated and the activity of the solvent controls (DMSO) was set as 100 %. All measurements were carried out at the room temperature as triplicates.

ALOX Activity Assay (bacterial lysate supernatants). Since mouse Alox15 is difficult to purify these comparative experiments were carried out with crude enzyme preparations. For this purpose the recombinant enzymes were expressed in *E. coli* and bacterial lysate supernatants were used as enzyme source. 2 to 10 µL of bacterial cell lysate supernatants were pre-incubated with 2 µM of 8b at 25° C for 1 min and the ALOX reaction was started by the addition of 25 µM AA or LA. After 3 min the reaction was stopped by addition of $NaBH_4$. Samples were acidified, proteins were precipitated by the addition of 0.5 ml of acetonitrile and the precipitate was spun down. The extent of the ALOX activity was measured by HPLC quantification of the ALOX products (13-HODE for LA oxygenation, sum of 12- + 15-HETE for AA oxygenation). For each inhibitor concentration measurements were carried out in triplicate.

Cellular ALOX Activity Assay. To test the impact of the novel ALOX inhibitors on the cellular activity of human ALOX15 we employed L1236 human Hodgkin lymphoma cell lines. These cells constitutively express native human ALOX15 at high levels[41]. In these experiments the cultured L1236 cells were pre-incubated in the absence or presence of different inhibitor concentrations (**8b** or ETYA) at 25 °C for 5 min (0.25 mL of PBS with 0.1 mill. cells in total) and then the ALOX15 reaction was started by the addition of 25 µM of either AA or LA. After 10 min the reaction was stopped and the amounts of eicosanoids formed from the two fatty acid substrates were quantified by HPLC. For LA oxygenation the formation of 13-HODE was quantified. For AA oxygenation we separately evaluated the formation of 12-HETE and 15-HETE as independent measures. The ALOX activity of the incubation sample lacking the inhibitor was set 100%. As suitable measure for the substrate selectivity of the inhibitory effect we calculated the ratios of residual activities of LA oxygenation *vs.* AA oxygenation.

Reversibility of inhibition. To test the reversibility of inhibition a solution of rabbit ALOX15 (3.3 µM) was pre-incubated in 1 mL phosphate buffer (pH 7.4) containing 300 µM (app. 100 molar excess) of the inhibitor for 2 min at 5 °C. The excess of inhibitor was removed by gel-filtration using a 1 mL PD MidiTrap 25-G column (GE Healthcare, Marlborough, USA). For this purpose, 1 mL of protein-inhibitor mixture was applied and the column was eluted with 2 mL of phosphate buffer (pH 7.4) according to the recommendation of the manufacturer. The column was washed and re-equilibrated with 50 mL of the elution buffer until no detectable traces of the inhibitor remained in the eluate. The procedure was repeated 3-4 times until the final ratio of a maximum of UV-absorbance at 318 nm (inhibitor specific chromophore) to the absorbance of protein (280 nm) remained constant. The amount of LOX protein left and that of the inhibitor bound was estimated spectrophotometricaly using molecular extinction coefficient ε=1,78 (mg^{-1} cm^{-1}) for LOX. The residual enzymatic activity was assayed spectrophotometrically comparing to the activity of the control (ALOX preparation without inhibitor).

Inhibitor recovery. Purified rabbit ALOX15 (10 µg) was pre-incubated with an aliquot of inhibitor **6-8** (10 µM final concentration) in 0.5 mL PBS for 1 min and the reaction was started by addition of 25 µM substrate. After 3 min the reaction was quenched with 0.5 mL of ice-cold methanol, the protein precipitate was spun down and aliquots of the clear supernatant (300µL) were injected for reverse-phase HPLC for quantification of the remaining inhibitor. For

each inhibitor concentration measurements were carried out in triplicate.

Molecular docking studies. Docking studies were carried out with the program GOLD5.8.0.[62] Concerning the **8a** and **8b** inhibitors, those calculations were restricted to the binding cavity of monomer A of rabbit ALOX15 considering the crystallographic x-ray structure of the dimeric enzyme (PDB entry 2PoM)[32] as the receptor. Before initiating the docking protocol, the ligand bound at the active site of the crystal structure was removed. Hydrogen coordinates were generated with the H++ web-server[63-64] using a pH 6.0 for titrable residues. By contrast, with AA and LA, the docking calculations were restricted to the binding cavity of monomer B of rabbit ALOX15 considering the relaxed ALOX15-8a(A)-empty(B) and ALOX15-8b(A)-empty(B) complexes as the receptors. The binding site cavity used in the docking runs is a 20 Å radius sphere centred around the iron atom of monomer A, when inhibitor **8a** or **8b** act as the ligand, or the iron atom of monomer B when AA or LA act as the ligand. The receptor was kept fixed but complete flexibility was given to the ligand in the conformational search. We activated the option in GOLD that considers the interactions of organic ligands with metal ions in metalloenzymes but limiting the docking exploration to hexacoordinated geometries of iron. The most efficient genetic algorithm was used to ensure an extensive search of the conformational space of all substrates. To estimate the binding free energies of substrates the ChemScore fitness function has been selected.

Molecular dynamics (MD) simulations. The system has been assembled using the recommended procedure by the AMBER program package.[65] The ff14SB[66] force field was used for the protein atoms. The force field parameters for AA,[67] LA[68] and iron and its first coordination sphere[42] (His361, His366, His541, His545, Ile 663 and OH^-) were taken from previous works while the specific parameters of **8a** and **8b** inhibitors were developed here. The calculations to generate those specific parameters were carried out following the standard protocol in AMBER with Antechamber and Parmchk2 modules even though, as both inhibitors are far from common substrates used with AMBER, a procedure developed by MacKerell et al.[69] had to be employed in order to overcome some large dihedral penalties. As the source for those parameters, the GAFF2[65, 70] library was used. The B3LYP/6-31G(d) level of theory was employed to optimize the **8a** and **8b** inhibitors' structures and their atomics charges were assigned using Merz-Kollman RESP procedure.[71] Besides, the protonation states for all ligands were established by hand to ensure that they match with the protonation state in physiological conditions.

All MD simulations followed the same protocol, the only differences are found in the length of the production period and the starting structures. After combing enzyme and substrate files, the different protein-substrate complexes were solvated with an orthorhombic box of pre-equilibrated TIP3P[72] waters and their total charge was neutralized by adding sodium cations using the tLeap program. The resulting systems contain nearly 200000 atoms being about 21000 of them of the protein. The remaining atoms represent water molecules and salt ions. All molecular dynamics (MD) simulations were run with AMBER 18 GPU (CUDA) version of the PMEMD package[73-74]. Initially, the systems were submitted to 22000 energy minimization steps using the steepest-descent method to avoid close contacts. In the first 6000 steps, harmonic restraints were applied to the protein and substrate atoms with a force constant of 5.0 kcal mol^{-1} $Å^{-2}$ so only the solvent and ions were relaxed. In the following 6000 steps, harmonic restraints were applied to the protein backbone and the substrate heavy atoms with a force constant again of 5.0 kcal mol-1 $Å^{-2}$. In the last 10000 steps the whole system was kept free of restraints. After that, MD simulations using periodic boundary conditions were carried out. The system was gradually heated from 0 K to 300 K for a period of 200 ps. Next, an MD run of 1 ns, at constant temperature and pressure (300 K, 1 bar), has been calculated to adjust the volume of the orthorhombic box so that a density of around 1 g cm^{-3} is reached. Throughout the heating and the compressing, harmonic restraints were applied to the protein backbone and substrate heavy atoms with a force constant of 5.0 kcal mol^{-1} $Å^{-2}$ whereas no restraints were applied to the rest of the system. The temperature was controlled by Langevin dynamics [75], while the pressure was adjusted by the Berendsen barostat[76]. Then, an equilibration stage of 10 ns, at constant temperature (300 K) and volume, was carried out. Finally, a production period was run within the same isothermal-isochoric ensemble. A time step of 2 fs was used along the whole MD trajectory. All bonds and bends containing hydrogen atoms were constrained by the SHAKE algorithm.[77] Non-bonding interactions have been calculated with a cut-off of 9 Å. The best docking pose of **8a** and **8b** into monomer A were used as the starting structure for the MD simulations of the ALOX15-**8a**(A)-empty(B) and ALOX15-**8b**(A)-empty(B) complexes, respectively. The length of the production period for those two MD trajectories was 200 ns for letting the system relax and adapt to the presence of the inhibitor. The last structures of those two MD simulations were then taken as receptors for docking AA and LA into monomer B of the ALOX15-8a(A)-empty(B) and ALOX15-8b(A)-emty(B) complexes. Next, the best docking pose of AA into monomer B was selected as the starting structure for the MD simulations of ALOX15-**8a**(A)-AA(B) and ALOX15-**8b**(A)-AA(B) as well as the best docking pose of LA that was taken to initiate the simulation of the ALOX15-**8a**(A)-LA(B) and ALOX15-**8b**(A)-LA(B) complexes. In these cases, a production period of 100 ns was run except for the ALOX15-**8a**(A)-LA(B) system that needed additional 100 ns to equilibrate. For the sake of comparison, we have also included the results of the MD simulation of the ALOX15-AA(B) complex (that is, without inhibitor) from our previous study.[42] Also, a 100 ns MD trajectory for the ALOX15-LA(B) system has been calculated here to compare with the simulations including an inhibitor and LA. The Leu183Glu+Leu192Glu mutant has been built using the CHIMERA[77] program from the wild-type $ALOX_{15}$ dimer

model. With the aim of relaxing the system in the presence of the double mutation, the length of the MD production period was 200 ns. Analysis of the MD simulations was carried out with AmberTools18, whereas visualization of those trajectories was performed with VMD[78] and USCF CHIMERA[79] programs. The cavity surfaces were calculated with the CavityPlus web server.[80]

SUPPORTING INFORMATION

- Dose response curves for all inhibitors tested, Michaelis–Menten plots at different inhibitor concentrations, inhibitor stability assays, impact of inhibitor on product specificity of ALOX15, docking studies and MD simulations of enzyme-inhibitor complexes, spectral and analytical data (^{1}H- and ^{13}C-NMR spectra, IR-spectra, UV-spectra, HRMS spectra, GC-MS- and HPLC-data) (PDF)
- Molecular string formulas (CSV)

AUTHOR INFORMATION

Corresponding Author

*Igor Ivanov – Lomonosov Institute of Fine Chemical Technologies, MIREA - Russian Technological University, Vernadskogo pr. 86, 119571 Moscow, Russia, orcid.org/0000-0003-0543-2067; E-mail: igor_ivanov@gmx.de; Tel: +7 (495) 246-05-55 (supl. 884)

Authors

#These authors equally contributed to the article

Author Contributions

I.I., H.K., J.M.L. and A.G.L designed the study. A.G, A.Z, R.S and V.A. performed synthesis and characterization of all compounds. I.I., A.Z, and K.R.K. carried out expression of the recombinant enzymes. I.I, A.Z and K.R.K. performed inhibitor testing and determined reaction specificity of the enzyme variants with polyenoic fatty acids. A.C. performed modelling and MD-simulations. I.I., A.G.L., J.M.L and H.K. drafted the manuscript and all authors contributed to prepare its final version.

Notes

Authors declare no competing financial interest.

ACKNOWLEDGMENT

Deutsche Forschungsgemeinschaft (KU 961/14-1), Russian Foundation for Basic Research (19-54-12002) and Russian Ministry of Science and High Education (0706-2020-0019) supported the experimental part of this work. We thank the Spanish "Ministerio de Ciencia, Innovación y Universidades" (Grant CTQ2017-83745-P). We also acknowledge CSUC for computational facilities and Shared Science and training Center for Collective Use of RTU MIREA. Authors also wish to thank Prof. Alexander V. Aksenov from North Caucasus Federal University (Russian Federation) for his valuable advises and comments regarding indole synthesis. Chemical synthesis of the inhibitors was carried out in the Ivanov lab in Moscow. Expression and purification of the recombinant enzymes, mutagenesis studies and the characterization experiments were carried out by I.I and his Russian colleagues during several sabbaticals in the Kühn lab in Berlin. *In silico* docking studies and MD simulations were performed in the González-Lafont lab in Barcelona.

REFERENCES

1. Cyrus, T.; Witztum, J. L.; Rader, D. J.; Tangirala, R.; Fazio, S.; Linton, M. F.; Funk, C. D., Disruption of the 12/15-lipoxygenase gene diminishes atherosclerosis in apo E-deficient mice. *J Clin Invest* **1999,** *103* (11), 1597-1604.
2. Pidgeon, G. P.; Lysaght, J.; Krishnamoorthy, S.; Reynolds, J. V.; O'Byrne, K.; Nie, D.; Honn, K. V., Lipoxygenase metabolism: roles in tumor progression and survival. *Cancer Metastasis Rev* **2007,** *26* (3-4), 503-524.
3. Cimen, I.; Tuncay, S.; Banerjee, S., 15-Lipoxygenase-1 expression suppresses the invasive properties of colorectal carcinoma cell lines HCT-116 and HT-29. *Cancer Sci* **2009,** *100* (12), 2283-2291.
4. Serhan, C. N.; Petasis, N. A., Resolvins and protectins in inflammation resolution. *Chem Rev* **2011,** *111* (10), 5922-5943.
5. Yoo, S.; Lim, J. Y.; Hwang, S. W., Resolvins: Endogenously-generated potent painkilling substances and their therapeutic perspectives. *Curr Neuropharmacol* **2013,** *11* (6), 664-676.
6. Ivanov, I.; Kuhn, H.; Heydeck, D., Structural and functional biology of arachidonic acid 15-lipoxygenase-1 (ALOX15). *Gene* **2015,** *573* (1), 1-32.
7. Pace, S.; Pergola, C.; Dehm, F.; Rossi, A.; Gerstmeier, J.; Troisi, F.; Pein, H.; Schaible, A. M.; Weinigel, C.; Rummler, S.; Northoff, H.; Laufer, S.; Maier, T. J.; Radmark, O.; Samuelsson, B.; Koeberle, A.; Sautebin, L.; Werz, O., Androgen-mediated sex bias impairs efficiency of leukotriene biosynthesis inhibitors in males. *J Clin Invest* **2017,** *127* (8), 3167-3176.
8. Larsen, J. S.; Acosta, E. P., Leukotriene-receptor antagonists and 5-lipoxygenase inhibitors in asthma. *Ann Pharmacother* **1993,** *27* (7-8), 898-903.
9. Mochizuki, N.; Kwon, Y. G., 15-lipoxygenase-1 in the vasculature: expanding roles in angiogenesis. *Circ Res* **2008,** *102* (2), 143-145.
10. Zhao, L.; Grosser, T.; Fries, S.; Kadakia, L.; Wang, H.; Zhao, J.; Falotico, R., Lipoxygenase and prostaglandin G/H synthase cascades in cardiovascular disease. *Expert Rev Clin Immunol* **2006,** *2* (4), 649-658.
11. Kapralov, A. A.; Yang, Q.; Dar, H. H.; Tyurina, Y. Y.; Anthonymuthu, T. S.; Kim, R.; St. Croix, C. M.; Mikulska-Ruminska, K.; Liu, B.; Shrivastava, I. H.; Tyurin, V. A.; Ting, H.-C.; Wu, Y. L.; Gao, Y.; Shurin, G. V.; Artyukhova, M. A.; Ponomareva, L. A.; Timashev, P. S.; Domingues, R. M.; Stoyanovsky, D. A.; Greenberger, J. S.; Mallampalli, R. K.; Bahar, I.; Gabrilovich, D. I.; Bayır, H.; Kagan, V. E., Redox lipid reprogramming commands susceptibility of macrophages and microglia to ferroptotic death. *Nat Chem Biol* **2020,** *16* (3), 278-290.
12. Kagan, V. E.; Mao, G.; Qu, F.; Angeli, J. P. F.; Doll, S.; Croix, C. S.; Dar, H. H.; Liu, B.; Tyurin, V. A.; Ritov, V. B.; Kapralov, A. A.; Amoscato, A. A.; Jiang, J.; Anthonymuthu, T.; Mohammadyani, D.; Yang, Q.; Proneth, B.; Klein-Seetharaman, J.; Watkins, S.; Bahar, I.; Greenberger, J.; Mallampalli, R. K.; Stockwell, B. R.; Tyurina, Y. Y.; Conrad, M.; Bayır, H., Oxidized arachidonic and adrenic PEs navigate cells to ferroptosis. *Nat Chem Biol* **2017,** *13* (1), 81-90.
13. de Luca, C.; Olefsky, J. M., Inflammation and insulin resistance. *FEBS Lett* **2008,** *582* (1), 97-105.
14. Sears, D. D.; Miles, P. D.; Chapman, J.; Ofrecio, J. M.; Almazan, F.; Thapar, D.; Miller, Y. I., 12/15-lipoxygenase is required for the early onset of high fat diet-induced adipose tissue inflammation and insulin resistance in mice. *PLoS One* **2009,** *4* (9), e7250.
15. Lieb, D. C.; Brotman, J. J.; Hatcher, M. A.; Aye, M. S.; Cole, B. K.; Haynes, B. A.; Wohlgemuth, S. D.; Fontana, M. A.; Beydoun, H.; Nadler, J. L.; Dobrian, A. D., Adipose tissue 12/15 lipoxygenase pathway in human obesity and diabetes. *J Clin Endocrinol Metab* **2014,** *99* (9), E1713-E1420.
16. Brinckmann, R.; Schnurr, K.; Heydeck, D.; Rosenbach, T.; Kolde, G.; Kühn, H., Membrane translocation of 15-lipoxygenase in hematopoietic cells is calcium-dependent and activates the oxygenase activity of the enzyme. *Blood* **1998,** *91* (1), 64-74.
17. Singh, N. K.; Rao, G. N., Emerging role of 12/15-Lipoxygenase (ALOX15) in human pathologies. *Prog Lipid Res* **2019,** *73*, 28-45.

18. Ackermann, J. A.; Hofheinz, K.; Zaiss, M. M.; Kronke, G., The double-edged role of 12/15-lipoxygenase during inflammation and immunity. *Biochim Biophys Acta* **2017,** *1862* (4), 371-381.
19. Zheng, Y.; Liu, Y.; Karatas, H.; Yigitkanli, K.; Holman, T. R.; van Leyen, K., Contributions of 12/15-Lipoxygenase to Bleeding in the Brain Following Ischemic Stroke. *Adv Exp Med Biol* **2019,** *1161*, 125-131.
20. Serhan, C. N.; Jain, A.; Marleau, S.; Clish, C.; Kantarci, A.; Behbehani, B.; Colgan, S. P.; Stahl, G. L.; Merched, A.; Petasis, N. A.; Chan, L.; Van Dyke, T. E., Reduced inflammation and tissue damage in transgenic rabbits overexpressing 15-lipoxygenase and endogenous anti-inflammatory lipid mediators. *J Immunol* **2003,** *171* (12), 6856-6865.
21. Il Lee, S.; Zuo, X.; Shureiqi, I., 15-Lipoxygenase-1 as a tumor suppressor gene in colon cancer: is the verdict in? *Cancer Metastasis Rev* **2011,** *30* (3-4), 481-491.
22. Rai, G.; Joshi, N.; Jung, J. E.; Liu, Y.; Schultz, L.; Yasgar, A.; Perry, S.; Diaz, G.; Zhang, Q.; Kenyon, V.; Jadhav, A.; Simeonov, A.; Lo, E. H.; van Leyen, K.; Maloney, D. J.; Holman, T. R., Potent and selective inhibitors of human reticulocyte 12/15-lipoxygenase as anti-stroke therapies. *J Med Chem* **2014,** *57* (10), 4035-4048.
23. Ngu, K.; Weinstein, D. S.; Liu, W.; Langevine, C.; Combs, D. W.; Zhuang, S.; Chen, X.; Madsen, C. S.; Harper, T. W.; Ahmad, S.; Robl, J. A., Pyrazole-based sulfonamide and sulfamides as potent inhibitors of mammalian 15-lipoxygenase. *Bioorg Med Chem Lett* **2011,** *21* (14), 4141-4145.
24. Weinstein, D. S.; Liu, W.; Ngu, K.; Langevine, C.; Combs, D. W.; Zhuang, S.; Chen, C.; Madsen, C. S.; Harper, T. W.; Robl, J. A., Discovery of selective imidazole-based inhibitors of mammalian 15-lipoxygenase: highly potent against human enzyme within a cellular environment. *Bioorg Med Chem Lett* **2007,** *17* (18), 5115-5120.
25. Sendobry, S. M.; Cornicelli, J. A.; Welch, K.; Bocan, T.; Tait, B.; Trivedi, B. K.; Colbry, N.; Dyer, R. D.; Feinmark, S. J.; Daugherty, A., Attenuation of diet-induced atherosclerosis in rabbits with a highly selective 15-lipoxygenase inhibitor lacking significant antioxidant properties. *Br J Pharmacol* **1997,** *120* (7), 1199-1206.
26. Barvian, N. C.; O'brian, P. M.; Patt, W. C.; Picard, J. A.; Sliskovic, D. R. 1,2,4-trisubstituted benzenes as inhibitors of 15-lipoxygenase. Patent WO 096298 A2, 20 December, 2001.
27. Connor, D.; Roark, W.; Sorenson, R. Indole and benzimidazole 15-lipoxygenase inhibitors. U.S. Patent 0038943 A1, February 26, 2004.
28. Eleftheriadis, N.; Neochoritis, C. G.; Leus, N. G.; van der Wouden, P. E.; Dömling, A.; Dekker, F. J., Rational development of a potent 15-lipoxygenase-1 inhibitor with in vitro and ex vivo anti-inflammatory properties. *J Med Chem* **2015,** *58* (19), 7850-7862.
29. Weinstein, D. S.; Liu, W.; Gu, Z.; Langevine, C.; Ngu, K.; Fadnis, L.; Combs, D. W.; Sitkoff, D.; Ahmad, S.; Zhuang, S.; Chen, X.; Wang, F. L.; Loughney, D. A.; Atwal, K. S.; Zahler, R.; Macor, J. E.; Madsen, C. S.; Murugesan, N., Tryptamine and homotryptamine-based sulfonamides as potent and selective inhibitors of 15-lipoxygenase. *Bioorg Med Chem Lett* **2005,** *15* (5), 1435-1440.
30. Ludwig, P.; Holzhutter, H. G.; Colosimo, A.; Silvestrini, M. C.; Schewe, T.; Rapoport, S. M., A kinetic model for lipoxygenases based on experimental data with the lipoxygenase of reticulocytes. *Eur J Biochem* **1987,** *168* (2), 325-337.
31. Shang, W.; Ivanov, I.; Svergun, D. I.; Borbulevych, O. Y.; Aleem, A. M.; Stehling, S.; Jankun, J.; Kuhn, H.; Skrzypczak-Jankun, E., Probing dimerization and structural flexibility of mammalian lipoxygenases by small-angle X-ray scattering. *J Mol Biol* **2011,** *409* (4), 654-668.
32. Choi, J.; Chon, J. K.; Kim, S.; Shin, W., Conformational flexibility in mammalian 15S-lipoxygenase: Reinterpretation of the crystallographic data. *Proteins* **2008,** *70* (3), 1023-1032.
33. Wecksler, A. T.; Kenyon, V.; Deschamps, J. D.; Holman, T. R., Substrate specificity changes for human reticulocyte and epithelial 15-lipoxygenases reveal allosteric product regulation. *Biochemistry* **2008,** *47* (28), 736473-75.
34. Wecksler, A. T.; Jacquot, C.; van der Donk, W. A.; Holman, T. R., Mechanistic investigations of human reticulocyte 15- and platelet 12-lipoxygenases with arachidonic acid. *Biochemistry* **2009,** *48* (26), 6259-6267.
35. Ivanov, I.; Cruz, A.; Zhuravlev, A.; Di Venere, A.; Nicolai, E.; Stehling, S.; Lluch, J. M.; González-Lafont, À.; Kuhn, H., Conformational heterogeneity and cooperative effects of mammalian ALOX15. *Int J Mol Sci* **2021,** *22* (6), 3285.
36. Gaikwad, R.; Bobde, Y.; Ganesh, R.; Patel, T.; Rathore, A.; Ghosh, B.; Das, K.; Gayen, S., 2-Phenylindole derivatives as anticancer agents: synthesis and screening against murine melanoma, human lung and breast cancer cell lines. *Synth Commun* **2019,** *49* (17), 2258-2269.
37. Aksenov, A. V.; Smirnov, A. N.; Aksenov, N. A.; Bijieva, A. S.; Aksenova, I. V.; Rubin, M., Benzimidazoles and benzoxazoles via the nucleophilic addition of anilines to nitroalkanes. *Org Biomol Chem* **2015,** *13* (14), 4289-4295.
38. Pigerol, C.; de Cointet de Fillain, P.; Nanthavong, S.; Le Blay, J. 2-Phenyl-indole derivatives and process for preparing the same. U.S. Patent 4,057,530, November 8, 1977.
39. Rai, G.; Joshi, N.; Perry, S.; Yasgar, A.; Schultz, L.; Jung, J. E.; Liu, Y.; Terasaki, Y.; Diaz, G.; Kenyon, V.; Jadhav, A.; Simeonov, A.; van Leyen, K.; Holman, T. R.; Maloney, D. J., Discovery of ML351, a potent and selective inhibitor of human 15-lipoxygenase-1. In *Probe Reports from the NIH Molecular Libraries Program*, National Center for Biotechnology Information (US): Bethesda (MD), 2010.
40. McGovern, S. L.; Caselli, E.; Grigorieff, N.; Shoichet, B. K., A Common mechanism underlying promiscuous inhibitors from virtual and high-throughput screening. *J Med Chem* **2002,** *45* (8), 1712-1722.
41. Claesson, H. E.; Griffiths, W. J.; Brunnström, A.; Schain, F.; Andersson, E.; Feltenmark, S.; Johnson, H. A.; Porwit, A.; Sjöberg, J.; Björkholm, M., Hodgkin Reed-Sternberg cells express 15-lipoxygenase-1 and are putative producers of eoxins in vivo: novel insight into the inflammatory features of classical Hodgkin lymphoma. *FEBS J* **2008,** *275* (16), 4222-4234.
42. Cruz, A.; Di Venere, A.; Mei, G.; Zhuravlev, A.; Golovanov, A.; Stehling, S.; Heydeck, D.; Lluch, J. M.; González-Lafont, À.; Kuhn, H.; Ivanov, I., A role of Gln596 in fine-tuning mammalian ALOX15 specificity, protein stability and allosteric properties. *Biochim Biophys Acta Mol Cell Biol Lipids* **2020,** *1865* (7), 158680.
43. Kühn, H.; Holzhütter, H. G.; Schewe, T.; Hiebsch, C.; Rapoport, S. M., The mechanism of inactivation of lipoxygenases by acetylenic fatty acids. *Eur J Biochem* **1984,** *139* (3), 577-583.
44. Ivanov, I.; Shang, W.; Toledo, L.; Masgrau, L.; Svergun, D. I.; Stehling, S.; Gomez, H.; Di Venere, A.; Mei, G.; Lluch, J. M.; Skrzypczak-Jankun, E.; González-Lafont, À.; Kuhn, H., Ligand-induced formation of transient dimers of mammalian 12/15-lipoxygenase: a key to allosteric behavior of this class of enzymes? *Proteins* **2012,** *80* (3), 703-712.
45. Kuhn, H.; Heydeck, D.; Sprecher, H., On the mechanistic reasons for the dual positional specificity of the reticulocyte lipoxygenase. *Biochim Biophys Acta* **1991,** *1081* (2), 129-134.
46. Vogel, R.; Jansen, C.; Roffeis, J.; Reddanna, P.; Forsell, P.; Claesson, H. E.; Kuhn, H.; Walther, M., Applicability of the triad concept for the positional specificity of mammalian lipoxygenases. *J Biol Chem* **2010,** *285* (8), 5369-5376.
47. Freedman, C.; Tran, A.; Tourdot, B. E.; Kalyanaraman, C.; Perry, S.; Holinstat, M.; Jacobson, M. P.; Holman, T. R., Biosynthesis of the maresin intermediate, 13S,14S-Epoxy-DHA, by human 15-lipoxygenase and 12-lipoxygenase and its regulation through negative allosteric modulators. *Biochemistry* **2020,** *59* (19), 1832-1844.
48. Meng, H.; Dai, Z.; Zhang, W.; Liu, Y.; Lai, L., Molecular mechanism of 15-lipoxygenase allosteric activation and inhibition. *Phys Chem Chem Phys* **2018,** *20* (21), 14785-14795.
49. Meng, H.; McClendon, C. L.; Dai, Z.; Li, K.; Zhang, X.; He, S.; Shang, E.; Liu, Y.; Lai, L., Discovery of novel 15-lipoxygenase activators to shift the human arachidonic acid metabolic network toward inflammation resolution. *J Med Chem* **2016,** *59* (9), 4202-4209.
50. Zhou, J.; Li, Q.; Wu, M.; Chen, C.; Cen, S., Progress in the rational design for polypharmacology drug. *Curr Pharm Des* **2016,** *22* (21), 3182-3189.
51. Yuan, C.; Rieke, C. J.; Rimon, G.; Wingerd, B. A.; Smith, W. L., Partnering between monomers of cyclooxygenase-2 homodimers. *Proc Natl Acad Sci U S A* **2006,** *103* (16), 6142-6147.
52. Hafner, A. K.; Cernescu, M.; Hofmann, B.; Ermisch, M.; Hornig, M.; Metzner, J.; Schneider, G.; Brutschy, B.; Steinhilber, D.,

Dimerization of human 5-lipoxygenase. *Biol Chem* **2011,** *392* (12), 1097-1111.

53. Tsai, W.-C.; Aleem, A. M.; Whittington, C.; Cortopassi, W. A.; Kalyanaraman, C.; Baroz, A.; Iavarone, A. T.; Skrzypczak-Jankun, E.; Jacobson, M. P.; Offenbacher, A. R.; Holman, T., Mutagenesis, hydrogen–deuterium exchange, and molecular docking investigations establish the dimeric interface of human platelet-type 12-lipoxygenase. *Biochemistry* **2021,** *60* (10), 802-812.

54. Burrall, B. A.; Cheung, M.; Chiu, A.; Goetzl, E. J., Enzymatic properties of the 15-lipoxygenase of human cultured keratinocytes. *J Invest Dermatol* **1988,** *91* (4), 294-297.

55. Di Venere, A.; Horn, T.; Stehling, S.; Mei, G.; Masgrau, L.; González-Lafont, À.; Kuhn, H.; Ivanov, I., Role of Arg403 for thermostability and catalytic activity of rabbit 12/15-lipoxygenase. *Biochim Biophys Acta* **2013,** *1831* (6), 1079-1088.

56. Bryant, R. W.; Bailey, J. M.; Schewe, T.; Rapoport, S. M., Positional specificity of a reticulocyte lipoxygenase. Conversion of arachidonic acid to 15-S-hydroperoxy-eicosatetraenoic acid. *J Biol Chem* **1982,** *257* (11), 6050-6055.

57. Kuhn, H.; Sprecher, H.; Brash, A. R., On singular or dual positional specificity of lipoxygenases. The number of chiral products varies with alignment of methylene groups at the active site of the enzyme. *J Biol Chem* **1990,** *265* (27), 16300-16305.

58. Chaturvedi, S. K.; Ma, J.; Brown, P. H.; Zhao, H.; Schuck, P., Measuring macromolecular size distributions and interactions at high concentrations by sedimentation velocity. *Nat Commun* **2018,** *9* (1), 4415.

59. Chaturvedi, S. K.; Sagar, V.; Zhao, H.; Wistow, G.; Schuck, P., Measuring ultra-weak protein self-association by non-ideal sedimentation velocity. *J Am Chem Soc* **2019,** *141* (7), 2990-2996.

60. Kozlov, N.; Humeniuk, L.; Ufer, C.; Ivanov, I.; Golovanov, A.; Stehling, S.; Heydeck, D.; Kuhn, H., Functional characterization of novel ALOX15 orthologs representing key steps in mammalian evolution supports the Evolutionary Hypothesis of reaction specificity. *Biochim Biophys Acta Mol Cell Biol Lipids* **2019,** *1864* (3), 372-385.

61. Ivanov, I.; Di Venere, A.; Horn, T.; Scheerer, P.; Nicolai, E.; Stehling, S.; Richter, C.; Skrzypczak-Jankun, E.; Mei, G.; Maccarrone, M.; Kuhn, H., Tight association of N-terminal and catalytic subunits of rabbit 12/15-lipoxygenase is important for protein stability and catalytic activity. *Biochim Biophys Acta* **2011,** *1811* (12), 1001-1010.

62. Jones, G.; Willett, P.; Glen, R. C.; Leach, A. R.; Taylor, R., Development and validation of a genetic algorithm for flexible docking. *J Mol Biol* **1997,** *267* (3), 727-748.

63. Anandakrishnan, R.; Aguilar, B.; Onufriev, A. V., H++3.0: automating pK prediction and the preparation of biomolecular structures for atomistic molecular modeling and simulations. *Nucleic Acids Res* **2012,** *40* (W1), W537-W541.

64. Gordon, J. C.; Myers, J. B.; Folta, T.; Shoja, V.; Heath, L. S.; Onufriev, A., H++: a server for estimating pK(a)s and adding missing hydrogens to macromolecules. *Nucleic Acids Res* **2005,** *33*, W368-W371.

65. Case, D. A.; Ben-Shalom, I. Y.; Brozell, S. R.; Cerutti, D. S.; Cheatham, I., T.E.; Cruzeiro, V. W. D.; Darden, T. A.; Duke, R. E.; Ghoreishi, D.; Gilson, M. K.; Gohlke, H.; Goetz, A. W.; Greene, D.; Harris, R.; Homeyer, N.; Izadi, S.; Kovalenko, A.; Kurtzman, T.; Lee, T. S.; LeGrand, S.; Li, P.; Lin, C.; Liu, J.; Luchko, T.; Luo, R.; Mermelstein, D. J.; Merz, K. M.; Miao, Y.; Monard, G.; Nguyen, C.; Nguyen, H.; Omelyan, I.; Onufriev, A.; Pan, F.; Qi, R.; Roe, D. R.; Roitberg, A.; Sagui, C.; Schott-Verdugo, S.; Shen, J.; Simmerling, C. L.; Smith, J.; Salomon-Ferrer, R.; Swails, J.; Walker, R. C.; Wang, J.; Wei, H.; Wolf, R. M.; Wu , X.; Xiao, L.; York, D. M.; Kollman, P. A. *AMBER 2018*, University of California: San Francisco, 2018.

66. Maier, J. A.; Martinez, C.; Kasavajhala, K.; Wickstrom, L.; Hauser, K. E.; Simmerling, C., ff14SB: Improving the accuracy of protein side chain and backbone parameters from ff99SB. *J Chem Theory Comput* **2015,** *11* (8), 3696-3713.

67. Tosco, P., A mechanistic hypothesis for the aspirin-induced switch in lipid mediator production by cyclooxygenase-2. *J Am Chem Soc* **2013,** *135* (28), 10404-10410.

68. Ivanov, I.; Golovanov, A. B.; Ferretti, C.; Canyelles-Niño, M.; Heydeck, D.; Stehling, S.; Lluch, J. M.; González-Lafont, À.; Kühn, H., Mutations of triad determinants changes the substrate alignment at the catalytic center of human ALOX5. *ACS Chem Biol* **2019,** *14* (12), 2768-2782.

69. Guvench, O.; MacKerell, A. D., Jr., Automated conformational energy fitting for force-field development. *J Mol Model* **2008,** *14* (8), 667-679.

70. Wang, J.; Wolf, R. M.; Caldwell, J. W.; Kollman, P. A.; Case, D. A., Development and testing of a general amber force field. *J Comput Chem* **2004,** *25* (9), 1157-1174.

71. Bayly, C. I.; Cieplak, P.; Cornell, W. D.; Kollman, P. A., A Well-behaved electrostatic potential based method using charge restraints for deriving atomic charges - the Resp model. *J Phys Chem-Us* **1993,** *97* (40), 10269-10280.

72. Jorgensen, W. L.; Chandrasekhar, J.; Madura, J. D.; Impey, R. W.; Klein, M. L., Comparison of simple potential functions for simulating liquid water. *J Chem Phys* **1983,** *79* (2), 926-935.

73. Salomon-Ferrer, R.; Gotz, A. W.; Poole, D.; Le Grand, S.; Walker, R. C., Routine microsecond molecular dynamics simulations with AMBER on GPUs. 2. Explicit solvent particle Mesh Ewald. *J Chem Theory Comput* **2013,** *9* (9), 3878-3888.

74. Le Grand, S.; Gotz, A. W.; Walker, R. C., SPFP: Speed without compromise-A mixed precision model for GPU accelerated molecular dynamics simulations. *Comput Phys Commun* **2013,** *184* (2), 374-380.

75. Leach, A. R., *Molecular Modeling: Principles and Applications* Eddison Wesley Longman Limited: Essex, England, 1996; p 595.

76. Berendsen, H. J. C.; Postma, J. P. M.; Vangunsteren, W. F.; Dinola, A.; Haak, J. R., Molecular-dynamics with coupling to an external bath. *J Chem Phys* **1984,** *81* (8), 3684-3690.

77. Ryckaert, J.; Ciccotti, G.; Berendsen, H., Numerical-integration of cartesian equations of motion of a system with contraints - molecular dynamics of n-alkanes. *J Comput Phys* **1977,** *23* (3), 327-341.

78. Humphrey, W.; Dalke, A.; Schulten, K., VMD: visual molecular dynamics. *J Mol Graph* **1996,** *14* (1), 33-8.

79. Pettersen, E. F.; Goddard, T. D.; Huang, C. C.; Couch, G. S.; Greenblatt, D. M.; Meng, E. C.; Ferrin, T. E., UCSF chimera - A visualization system for exploratory research and analysis. *J Comput Chem* **2004,** *25* (13), 1605-1612.

80. Xu, Y.; Wang, S.; Hu, Q.; Gao, S.; Ma, X.; Zhang, W.; Shen, Y.; Chen, F.; Lai, L.; Pei, J., CavityPlus: a web server for protein cavity detection with pharmacophore modelling, allosteric site identification and covalent ligand binding ability prediction. *Nucleic Acids Res* **2018,** *46* (W1), W374-W379.

Table of Contents graphic

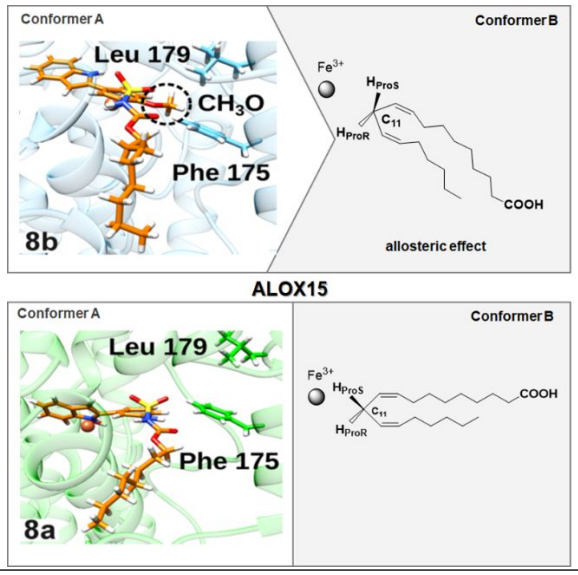

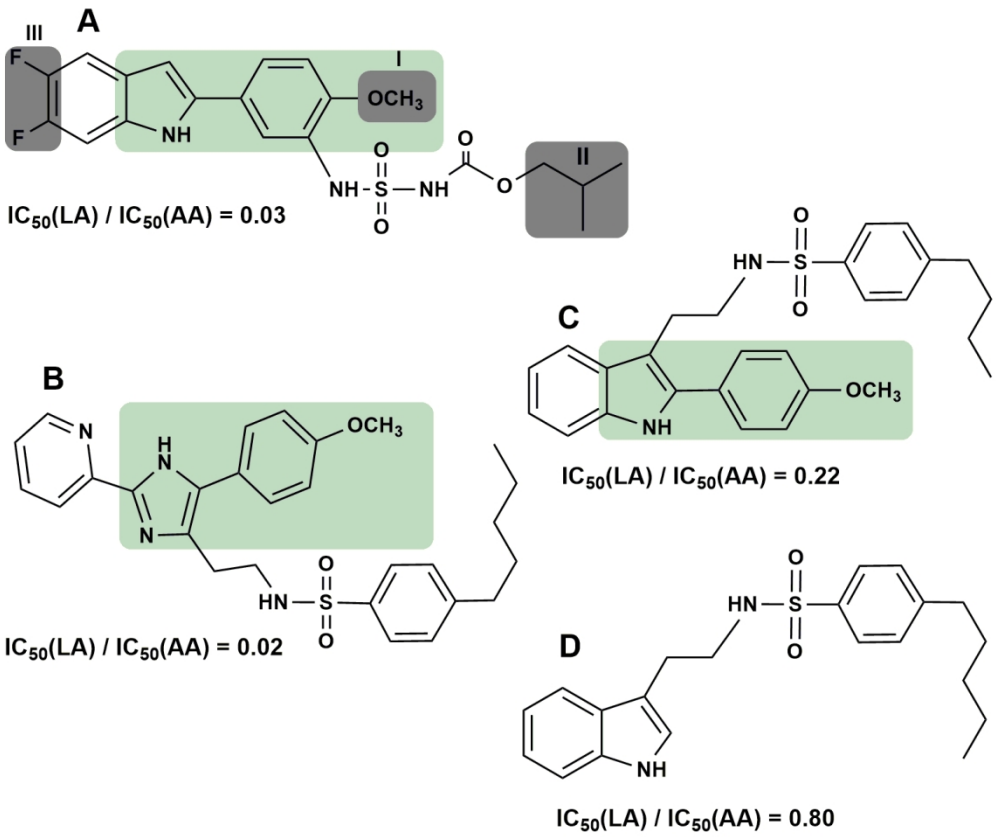

Figure 1. Selected structures of the substrate specific and non-specific ALOX15 inhibitors

133x111mm (300 x 300 DPI)

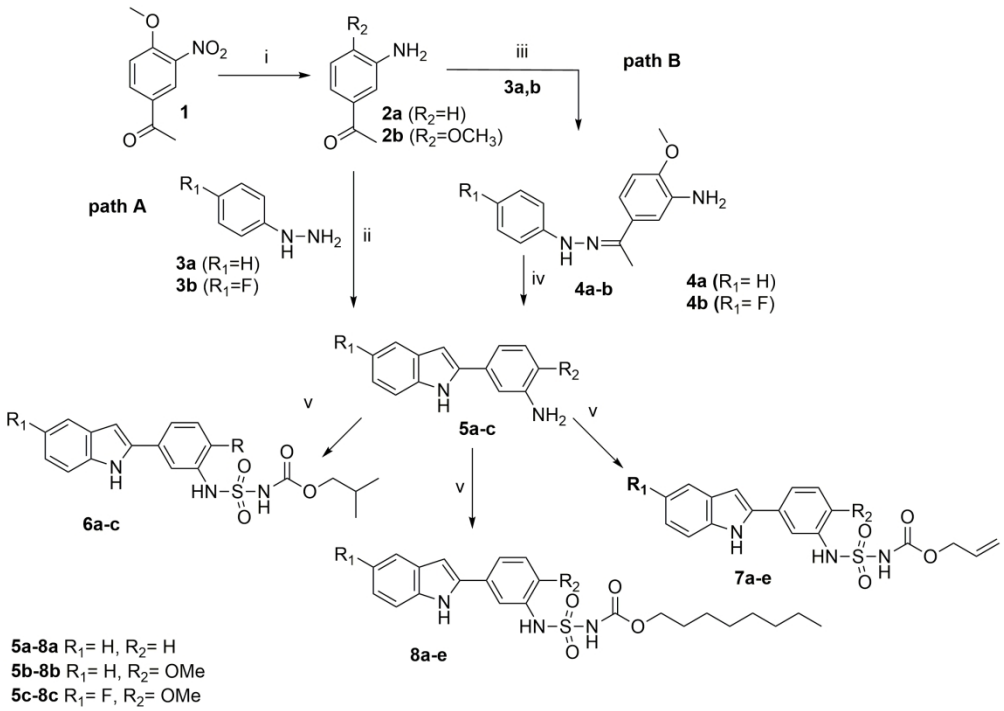

Scheme 1. Synthetic Route of compounds 6-8. Reagents and conditions: (i) 10% Pd/C, HCOONH4, EtOH, reflux; (ii) PPA, 130 oC, 0.5h; (iii) AcOH, EtOH, reflux; (iv) ZnCl2,180 oC, 2h; (v) ClSO2NCO, HN(C2H5)2, isobuthyl-, allyl - or octylalcohol, rt.

226x160mm (300 x 300 DPI)

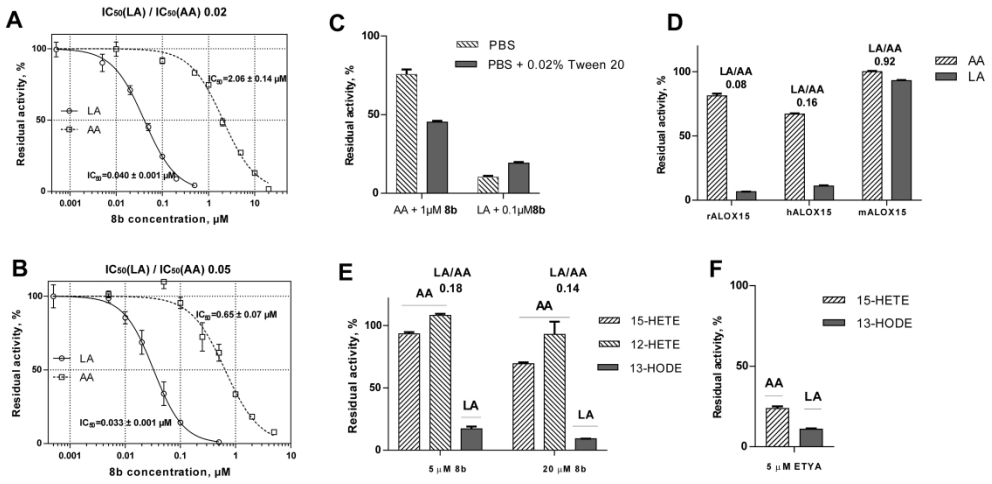

Figure 2. Dose response curves for inhibition of LA- and AA-oxygenase activities of mammalian ALOX15 orthologs. The LA- and AA oxygenase activities of pure recombinant rabbit (A) and pure recombinant human (B) ALOX15 orthologs were assayed in the presence or absence of compound 8b. Spectrophotometric assay were performed a described in Experimental Section and half-maximal inhibitory concentrations (IC50) were determined. (C) Effect of the detergent on inhibitory potency of 8b in rabbit ALOX15 assay. Spectrophotometric assay was performed a described in Experimental Section. (D) Inhibition of different mammalian ALOX15 orthologs by 8b using HPLC-based assay. The assay was performed a described in Experimental Section .The ALOX activity of the incubation sample lacking the inhibitor was set 100%. Finally, we calculated the ratios of residual activities of LA oxygenation vs. AA oxygenation (formation of 13-HODE vs. 15-HETE) as suitable measure for the substrate selectivity of the inhibitory effect. (E) Inhibition of the intracellular human ALOX15 by 8b using L1236 Hodgkin lymphoma cells. The assay was performed a described in Experimental Section. The ALOX activity of the incubation sample lacking the inhibitor was set 100%. As suitable measure for the substrate selectivity of the inhibitory effect of 8b we calculated the ratios of residual activities of LA oxygenation vs. AA oxygenation (formation of 13-HODE vs. 15-HETE). (F) Inhibition of the intracellular human ALOX15 by 5µM ETYA using L1236 Hodgkin lymphoma cells. The assay was performed under strictly comparable con-ditions as described for compound 8b. All data represent means ± SEM of n=3 measurements.

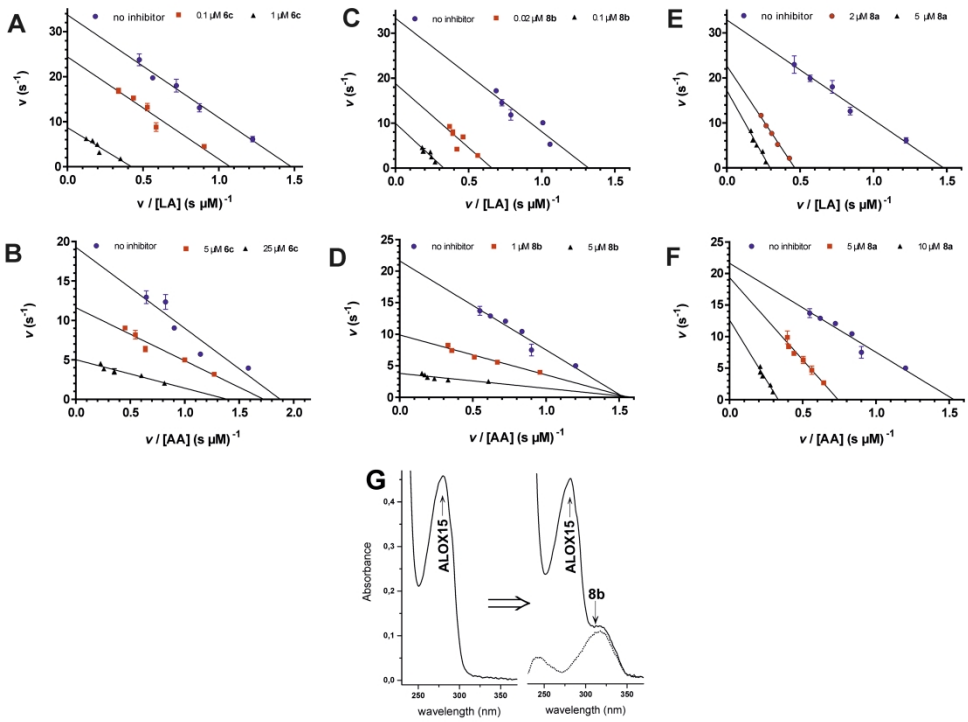

Figure 3. Mechanism of ALOX15 inhibition. (A-F) Eadie-Hofstee plots demonstrating the effects of 6c, 8b and 8a on rabbit ALOX15 when incubated with 25 μM linoleic (A, C, E) or arachidonic (B, D, F) acids. Incubations were repeated at different inhibitor concen-trations. All data points represent means ± SEM with n=3. (G) On average 1 molecule of 8b binds to 1 molecule of rabbit ALOX15. To estimate the rALOX15:8b ratio molecular extinction coefficient of 1.78 mg-1cm-1 (280 nm) for the enzyme was used.

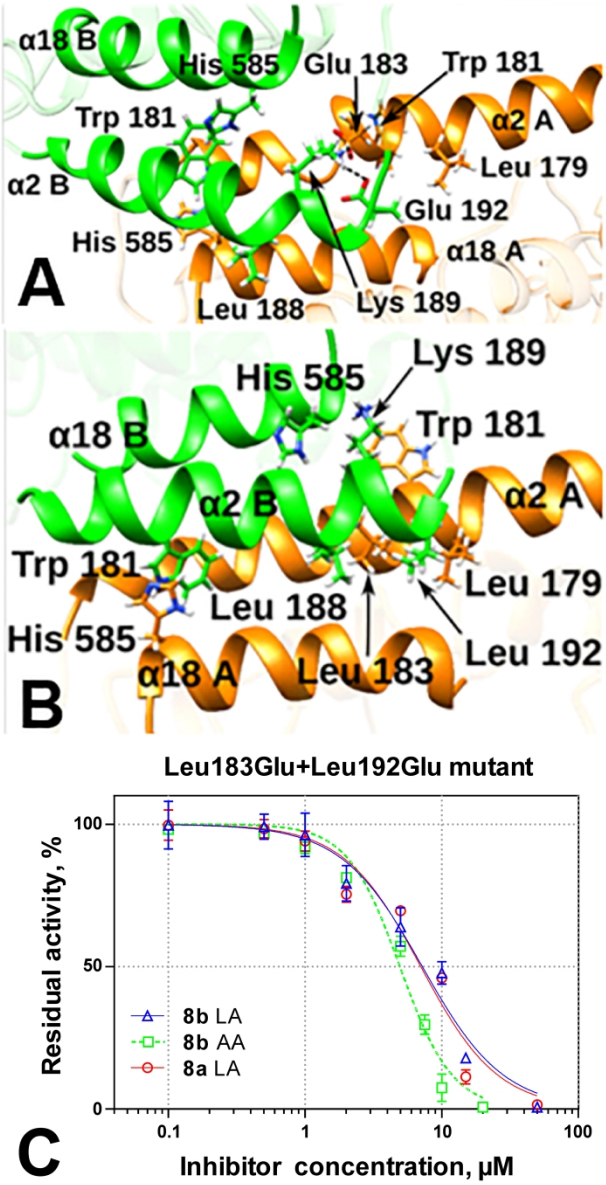

Figure 4. Leu183Glu+Leu192Glu mutant interface (A) vs. that of the wild-type enzyme (B). (C) Inhibition of linoleate and arachidonate oxygenase activity of rabbit ALOX15 L183E+L192E mutant (10 μg purified enzyme, 15 μM LA) in the presence of 8a and 8b. Spectrophotometric assays were performed as described in Experimental section. PDB ID 2P0M of crystal structures of rabbit ALOX15 was used as starting points for molecular modeling.

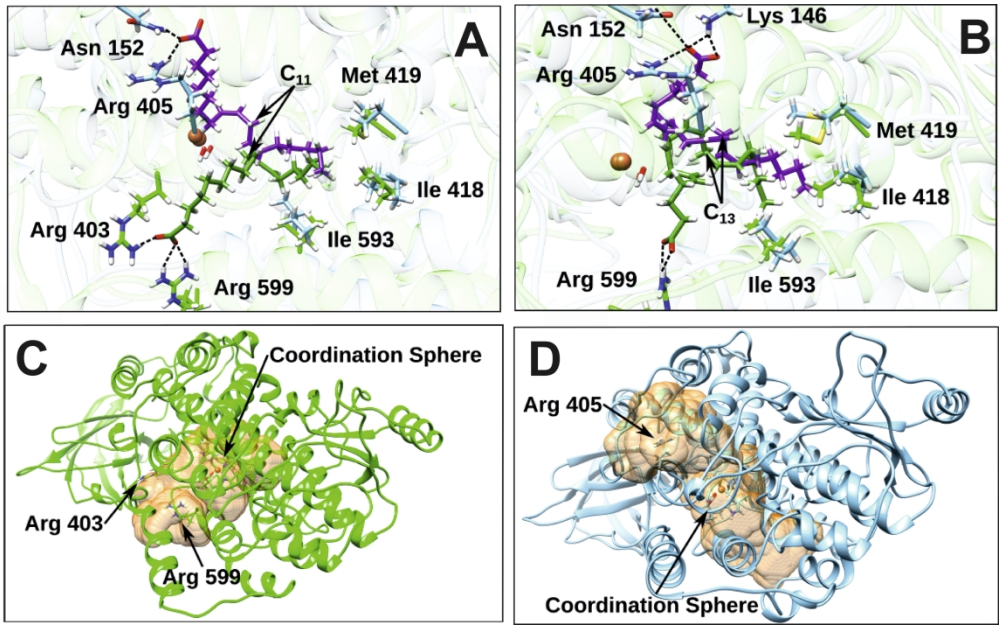

Figure 5. Effect of inhibitor on the substrate binding. (A) Most representative binding mode of LA in the ALOX15-8a(A)-LA(B) (in green) and ALOX15-8b(A)-LA(B) (in purple) complexes. (B) Most representative binding mode of AA in the ALOX15-8a(A)-AA(B) (in green) and ALOX15-8b(A)-AA(B) (in purple) complexes. The centroids of the most representative cluster for LA of the ALOX15-8a(A)-LA(B) and ALOX15-8b(A)-LA(B) complex simulations and for AA of the ALOX15-8a(A)-AA(B) and ALOX15-8b(A)-AA(B) complex simulations are depicted. The clustering has been carried out using an RMSD of 0.5 Å for the heavy atoms of the LA (AA) substrate. (C) Cavity surfaces of monomer B in ALOX15-8a(A)-LA(B) and (D) ALOX15-8b(A)-LA(B) complexes. Plots were carried out with the CavityPlus web server.

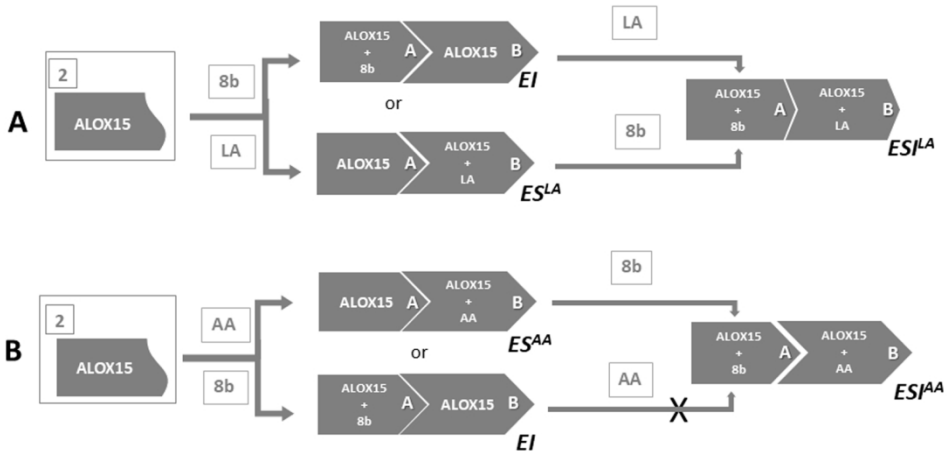

Figure 6. Schematic representation of the mechanism of proposed for action of 8b.

150x73mm (300 x 300 DPI)

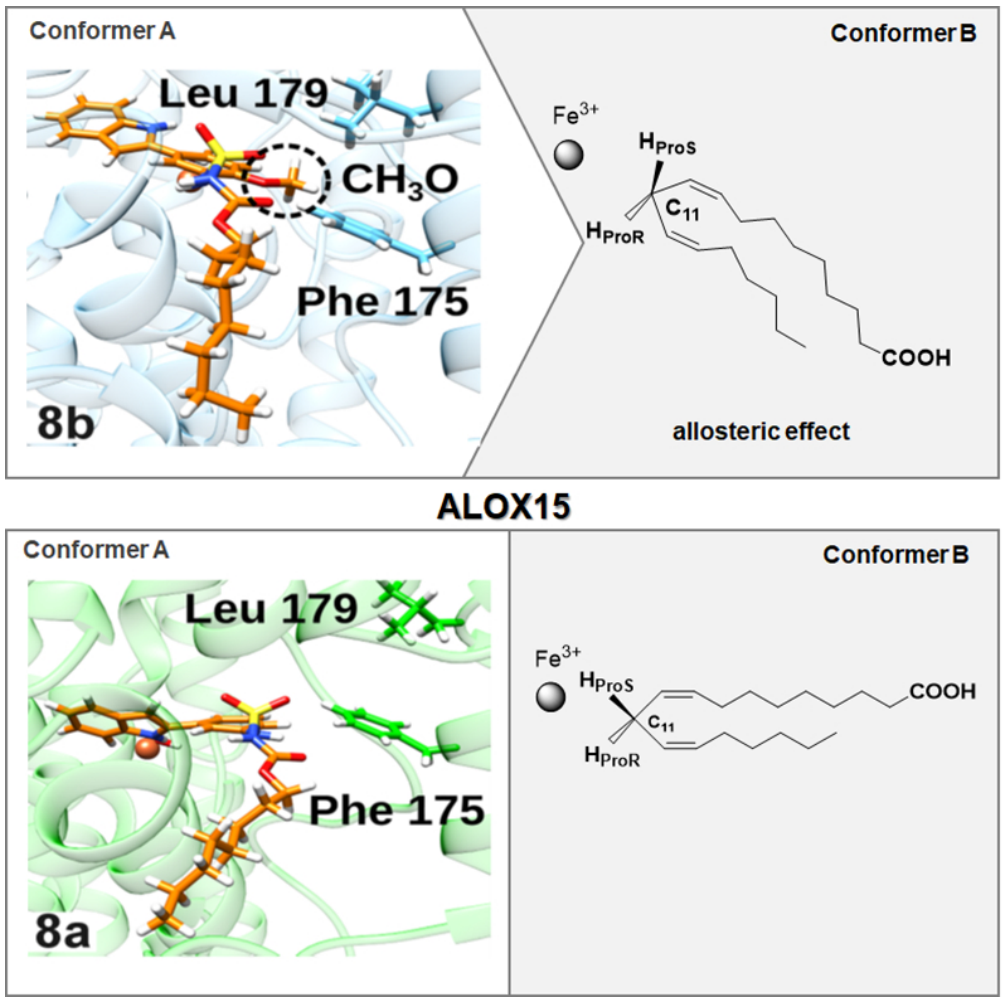

Table of Contents graphic

50x49mm (400 x 400 DPI)